The Effects of Retrograde Reactions and of Diffusion on ^{40}Ar–^{39}Ar Ages of Micas

J. ALLAZ[1], M. ENGI[1], A. BERGER[1,2] AND I. M. VILLA[1,3]

[1]INSTITUT FÜR GEOLOGIE, UNIVERSITÄT BERN, BALTZERSTRASSE 3, 3012 BERN, SWITZERLAND

[2]INSTITUT FOR GEOGRAFI OG GEOLOGI, KØBENHAVNS UNIVERSITET, ØSTER VOLDGADE 10, 1350 COPENHAGEN, DENMARK

[3]DIPARTIMENTO DI SCIENZE GEOLOGICHE E GEOTECNOLOGIE, UNIVERSITÀ DI MILANO BICOCCA, 20126 MILANO, ITALY

RECEIVED AUGUST 19, 2009; ACCEPTED DECEMBER 28, 2010
ADVANCE ACCESS PUBLICATION FEBRUARY 15, 2011

The effects of metamorphic reactions occurring during decompression were explored to understand their influence on the ^{40}Ar–^{39}Ar ages of micas. Monometamorphic metasediments from the Lepontine Alps (Switzerland) reached lower amphibolite facies during the Barrovian metamorphism related to the collision between European and African (Adria) continental plates. Mineral assemblages typically composed of garnet, plagioclase, biotite, muscovite and paragonite (or margarite) were screened for petrological equilibrium, to focus on samples that record a minimum degree of retrogression. X-ray diffraction data indicate that some mineral separates prepared for ^{40}Ar–^{39}Ar stepwise heating analysis are monomineralic, whereas others are composed of two white micas (muscovite with paragonite or margarite), or biotite and chlorite. In monomineralic samples $^{37}Ar/^{39}Ar$ and $^{38}Ar/^{39}Ar$ (proportional to Ca/K and Cl/K ratios) did not change and the resulting ages can be interpreted unambiguously. In mineral separates containing two white micas, Ca/K and Cl/K ratios were variable, reflecting non-simultaneous laboratory degassing of the two heterochemical Ar reservoirs. These ratios were used to identify each Ar reservoir and to unravel the age. In a chlorite–margarite–biotite calcschist equilibrated near 560°C and 0·65 GPa, biotite, margarite, and muscovite all yield ages around 18 Ma. At slightly higher grade (560–580°C, 0·8–0·9 GPa), the assemblage muscovite–paragonite–plagioclase is in equilibrium and remains stable during retrogression. In this case, muscovite and paragonite yield indistinguishable ages around 16·5 Ma. Above 590°C, paragonite was mostly consumed to form plagioclase >590°C, whereby the relict mica yields an age up to 5·6 Ma younger than muscovite. This partial or total resetting of the Ar clock in paragonite is interpreted to reflect plagioclase growth during decompression. Where biotite is present within this same assemblage, it systematically yields a younger age than muscovite, by 0·5–2 Ma. However, these biotites all show small amounts of retrograde chlorite formation. We conclude that even very minor chloritization of biotite is apparently a more effective process than temperature in resetting the Ar clock, as is the formation of plagioclase from paragonite decomposition. Multi-equilibrium thermobarometry is an excellent means to ensure that equilibrium in investigated samples is preserved, and this helps to obtain geologically meaningful metamorphic ages. However, even samples passing such equilibrium tests may still show retrograde effects that affect the Ar retention of micas. A more robust interpretation of such ^{40}Ar–^{39}Ar results may require use of a second geochronometer, such as U–Pb on monazite.

KEY WORDS: *^{40}Ar–^{39}Ar dating; metamorphic reactions; retrogression; metapelite; closure temperatures; Central Alps*

INTRODUCTION

Geochronology is the science of dating a geological process. In the context of ^{40}Ar–^{39}Ar geochronology, the dating result should reflect the crystallization age (i.e. the time of mineral growth), provided no loss or gain of the radiogenic isotopes has occurred. Loss or gain of isotopes occurs owing to (1) diffusive re-equilibration, (2) metamorphic reaction and/or recrystallization, or (3) inheritance. Jäger *et al.* (1967) originally proposed the concept of closure temperature based on diffusion theory and applied it to Rb–Sr dating of micas from basement gneisses in the Central Alps [case (1)]. Her empirical estimates for

*Corresponding author. Present address: Department of Geosciences, University of Massachusetts, 611 North Pleasant Street, Amherst, MA 01003-9297, USA. E-mail: jallaz@geo.umass.edu

K–Ar closure temperatures were 300°C for biotite and 350°C for muscovite (Purdy & Jäger, 1976). These closure temperature values have been less commonly used in the last 20 years. However, simple diffusion theory explicitly excludes retrograde mineral reactions, which are expected to induce isotopic resetting (e.g. Chopin & Maluski, 1980; Wijbrans & McDougall, 1986; Villa, 1998*b*, 2010; Di Vincenzo *et al.*, 2004; Gouzu *et al.*, 2006; Glodny *et al.*, 2008*a*, 2008*b*).

We decided to re-examine the mica ^{40}Ar–^{39}Ar ages in the same area where Jäger carried out her classic studies, but now selecting petrologically well-characterized samples, constrained by careful thermobarometry. We focused on the effects of late recrystallization during retrogression [case (2)], which was not taken into account 40 years ago. To avoid the problem of inheritance [case (3)], care was taken to study texturally and chemically well-equilibrated metasediments affected by a single metamorphic event. Chemical equilibration can be assessed by using thermobarometry. Where a well-equilibrated assemblage is preserved, all mineral equilibria computed with TWQ (Berman, 1991) should intersect at a single point. Moreover, mineral assemblages modelled with THERIAK-DOMINO (de Capitani & Petrakakis, 2010) should be consistent with both the observed mineral assemblage and the analysed mineral compositions. In selecting samples for this study, we ensured that the pressure (P) and temperature (T) conditions of equilibrium were tightly constrained, so as to minimize the chance of inheritance in the form of detrital mica. By comparing the reults of THERIAK-DOMINO modelling with the observed mineral assemblage, composition and texture, the possible mineral reactions occurring near the thermal peak and during the decompression and retrogression path were identified. The use of phase diagrams depicting the evolution of assemblages and the changes in mineral composition involved was necessary to ascertain the state of equilibrium of a specific mineral assemblage. Such diagrams also helped us identify the phases that may have been involved in retrograde reactions and thus were susceptible to chemical re-equilibration (e.g. chloritization, mineral resorption, late mineral growth).

We explored the effects of late chloritization of biotite and the breakdown of paragonite related to plagioclase growth, and specifically their effect on Ar retention. The interpretation of ^{40}Ar–^{39}Ar ages obtained for mixtures (muscovite–paragonite and muscovite–margarite) was also investigated, which required meticulous characterization of each mineral separate analysed. Although the K concentrations of paragonite and margarite are low, we tested whether it is possible to obtain meaningful ages for these micas as well. A detailed examination of these ages with regard to petrography and tightly constrained P–T results appears as a necessary step for sound geological interpretations.

GEOLOGICAL SETTING

The tectono-metamorphic history of the Central (or Lepontine) Alps is well known (e.g. Frey, 1969; Trommsdorff, 1980; Todd & Engi, 1997; Frey & Ferreiro Mählmann, 1999), and therefore this area was selected for the present study. The observed Barrovian metamorphic field gradient resulted from the collision of the European with the African plate. From north to south, the metamorphic grade increases regularly, from non-metamorphic and anchimetamorphic fields in the Jura and the Prealps Mountains up to the greenschist and finally amphibolite facies in the Central Alps. The latter is a flat-lying belt delimited by the Northern and Southern Steep Belts (NSB, SSB; Fig. 1a; Milnes, 1974). The frontal part of the Central Alps is delimited to the north by polymetamorphic gneiss units of the Aar massif and the Gotthard crystalline nappe, to the south by Sub-Pennine basement nappes (Fig. 1a; Berger *et al.*, 2005). According to Schmid *et al.* (1996) and Pfiffner *et al.* (2000), this part of the Alpine orogeny followed a collisional stage, during which the combined effects of extension, back-thrusting and fast erosion led to rapid exhumation.

Samples were collected in the northern Lepontine metamorphic dome, exclusively from Mesozoic metasediments, essentially in the Quartenschiefer (upper Triassic) and the base of the Bündnerschiefer unit (lower Liassic; Probst, 1980). The Quartenschiefer are typical Al-rich metapelites, whereas the Bündnerschiefer are calcschists generally rich in organic material. In the area studied, organic material has evolved to graphite as a result of the increase in metamorphic grade (Beyssac *et al.*, 2002; Petrova *et al.*, 2002). The Gotthard nappe and surrounding metasediments reached greenschist facies in Alpine times, whereas the Mesozoic metasediments further south attained lower amphibolite facies. This progressive transition is clearly displayed by the mineral assemblages in the metasediments (see review by Frey & Ferreiro Mählmann, 1999). Of special importance for this study is the occurrence of margarite and paragonite. Together with carbonate and epidote, they reacted to form prograde plagioclase in the area of interest, and are consumed entirely in samples from middle to upper amphibolite facies (Frey & Niggli, 1972; Frey & Orville, 1974; Frey *et al.*, 1982; Bucher-Nurminen *et al.*, 1983; Frank, 1983; Livi *et al.*, 2002). Previous TWQ thermobarometry by Todd & Engi (1997) found P–T conditions around 0·55–0·60 GPa and 550–600°C.

SAMPLE DESCRIPTION

Two to three samples from each of four areas were selected for the present study (Fig. 1b). Samples were selected based on their apparent textural equilibrium, which is characterized by the absence of retrograde phases and the well-preserved mineral assemblage reflecting the peak of

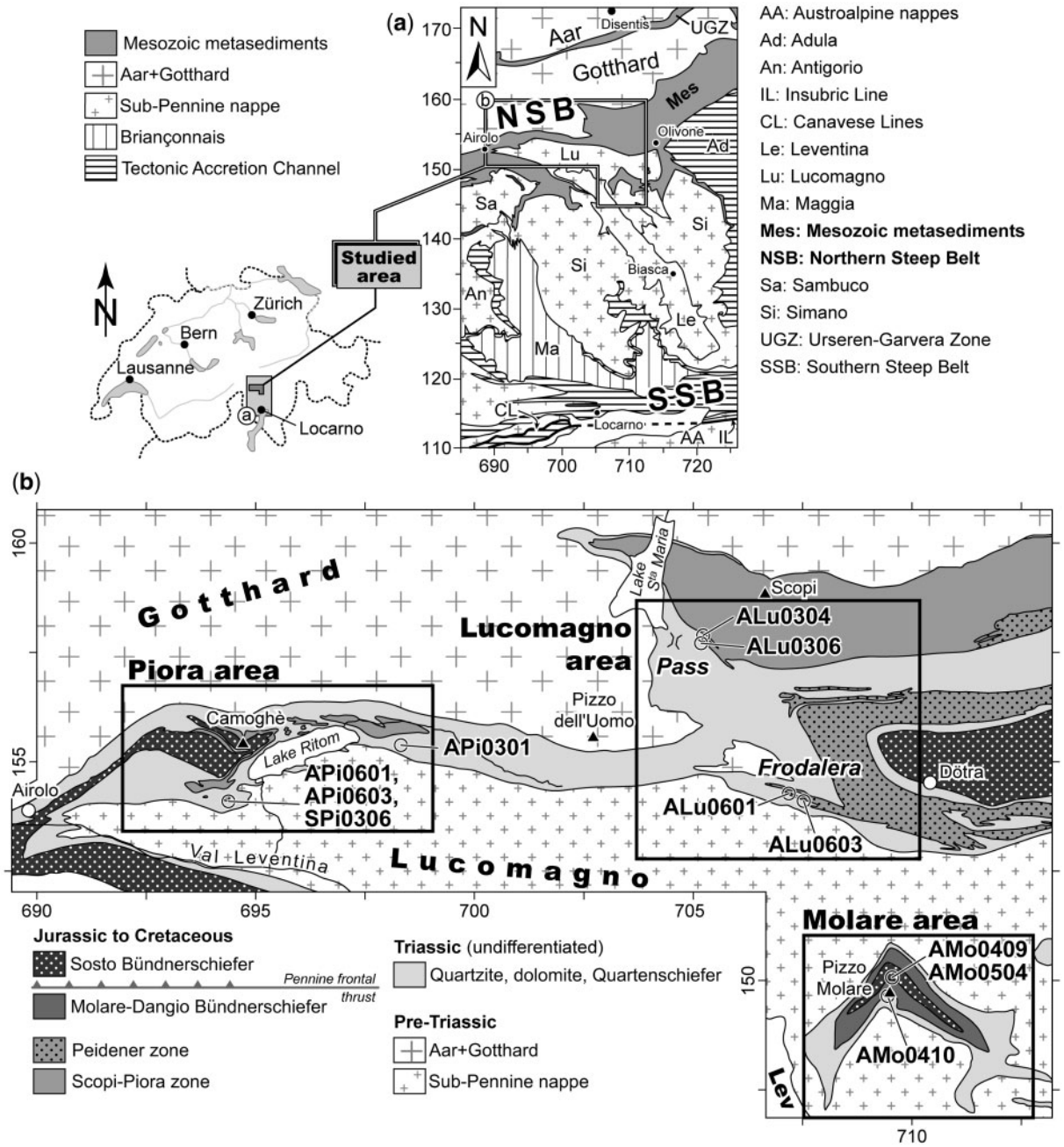

Fig. 1. (a) Geological overview of the Central Alps according to Spicher (1972) and Berger *et al.* (2005). (b) Geological map of the study area adapted from Probst (1980). Open circles indicate sample locations. Geographical coordinates are Swiss topographic map coordinates (in km).

metamorphism. From lowest to highest grade, the areas were: Lucomagno Pass, Frodalera (SE Lucomagno), Piora and Molare. Metapelites and metamarls were the most advantageous samples for the purpose of this study for several reasons: (1) the prograde mineral evolution of these samples at the beginning of the amphibolite facies included several net-transfer reactions and many of them involved devolatilization, which promoted pervasive equilibration as reflected by precise thermobarometric data; (2) large amounts of mica were produced in rocks of such Al-rich bulk composition, making sample preparation for ^{40}Ar–^{39}Ar dating easier; (3) the danger of inheritance of a pre-Alpine component in the mica samples is minimal, as their sedimentary protoliths were post-Variscan and

were affected by a single metamorphic event. Previous work by Hammerschmidt & Frank (1991) demonstrated that the detrital Ar signature in micas disappears completely at $T > 500°C$. This ensures that we dated thoroughly recrystallized samples that exclusively reflect mid-Tertiary Alpine metamorphism.

Lucomagno Pass

ALu0304 and ALu0306 are metamarls from the Quartenschiefer collected at the base of the Scopi Bündnerschiefer (Fig. 1b; Baumer *et al.*, 1961). Both samples mark the transition from greenschist to epidote-amphibolite facies. Fine flakes of margarite and rare to minor muscovite occur in both samples, forming thin layers that alternate with quartz (ALu0304) or quartz and carbonate (ALu0306, Fig. 2a). Grain sizes for micas are given in Table 1. ALu0306 is rich in carbonate (ankerite), contains abundant light green to colourless chlorite, brownish green biotite and clinozoisite, all aligned in the foliation. Chlorite is found both as large millimetre-sized flakes and finer interlayered grains with biotite (Fig. 2a). ALu0304 is more siliciclastic and contains brown biotite, large idioblastic garnet, and rare clinozoisite. Carbonate in this sample was exclusively found as inclusions in garnet. The very first plagioclase appears in these lithologies, either forming small, sparse grains in the matrix (ALu0304 and ALu0306; Fig. 2a) or millimetre-sized neoblasts overgrowing the schistosity (ALu0306). The growth of plagioclase is related to partial breakdown of margarite, as indicated by the close spatial relation between the two minerals (Fig. 2a).

Frodalera and Piora

The graphitic schists from Frodalera are from the base of the Scopi Bündnerschiefer (ALu0601, ALu0603), whereas those from Piora are graphite-free Quartenschiefer (APi0301, APi0601, APi0603; Fig. 1b). These samples are Al-rich metapelites; quartz and micas are the dominant phases. Muscovite typically coexists with paragonite and, owing to the variable Na and K contents of the bulk-rocks (Supplementary Data Table 1, available at http://www.petrology.oxfordjournals.org), the modal proportion of the two white micas is highly variable, from solely muscovite (ALu0601) to a paragonite-rich assemblage (APi0601), with similar modes in the other samples (Fig. 2b). Single crystals of paragonite are usually smaller than muscovite, but typically form clusters up to 1 mm in length (Table 1). Biotite is fairly abundant in APi0601 and -03, and forms millimetre-sized flakes along the schistosity coexisting with oblique biotite books. In samples from Frodalera, biotite is scarce and grows as isolated flakes in the matrix or more commonly as small flakes around garnet. This latter feature indicates minor garnet resorption (ALu0601, -03; Fig. 2c). Large millimetre- to centimetre-sized garnet is always present together with common sub-idiomorphic and poikiloblastic staurolite and/or kyanite (Fig. 2c). Al-rich silicates overgrow the schistosity. APi0601, –03 and ALu0601 are noticeably richer in kyanite, whereas ALu0603 and APi0301 are richer in staurolite, with and without kyanite, respectively. Chlorite is stable in APi0601 only (Mg-richer metapelite), where it is interlayered at the micrometre scale with paragonite and is included in biotite (Fig. 2d). Ovoid blasts of plagioclase are elongate in the schistosity (Fig. 2d) and include all matrix minerals, notably biotite, white micas, quartz and epidote.

Molare

Samples from this area are metapelites from the Quartenschiefer. They are composed of quartz, white mica, biotite, garnet, plagioclase and minor staurolite (AMo0409, –10), in AMo0410 with kyanite. Garnet-rich layers alternate with biotite-rich layers in AMo0410 (Fig. 2e), reflecting changes in Mn and Ca contents (MnO from 3% to <1%; CaO from 3% to 2%). In AMo0410 scarce paragonite occurs in apparent textural equilibrium with muscovite and plagioclase. At higher T (i.e. further south) paragonite is absent in metapelite assemblages, and only muscovite remains stable. Margarite is found in garnet cores, suggesting the former coexistence of three white micas along the prograde path. This is consistent with observations further north, in samples from Urseren–Garvera Zone (Fig. 1a; Frey, 1969; Livi *et al.*, 1997, 2008).

ANALYTICAL METHODS

Bulk-rock and mineral analysis

Bulk-rock compositions were obtained by X-ray fluorescence (XRF) on glass pellets at the Institut des Géosciences, Université de Fribourg (Switzerland). Mineral analyses were obtained using either a CAMECA SX-50 or a JEOL-8200 electron microprobe (EMP) at the Institut für Geologie, Universität Bern. Results from the two instruments overlap within error. In both cases, wavelength-dispersive analysis (15 kV and 20 nA) was performed, and a minimum beam size (*c.* 1 μm) was used for garnet and staurolite. To minimize volatilization of alkalis, plagioclase and micas were analysed using a defocused beam (5–10 μm depending on grain size). Averaged analyses for white micas, biotite, chlorite, staurolite, garnet, and plagioclase are listed in Supplementary Data Table 1, together with the list of standards used. At least 3–5 analyses were obtained on each grain to check for homogeneity. Particular care was taken for micas used in dating, with usually more than 20 analyses from a minimum of five mica flakes per thin section. Analytical traverses were made in zoned minerals, notably plagioclase and garnet.

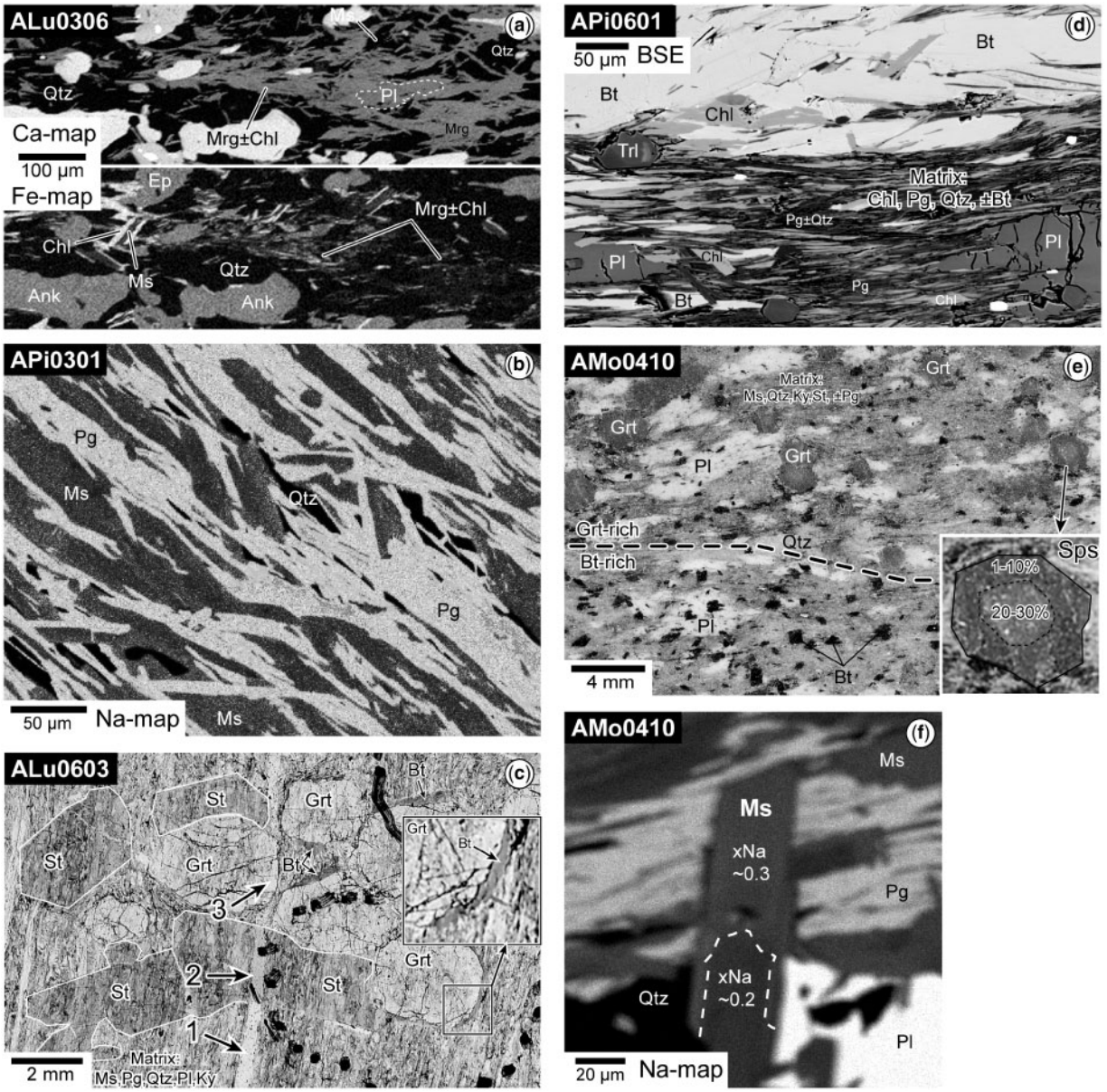

Fig. 2. (a) Ca and Fe element mapping showing occurrence of margarite and minor muscovite in metamarl ALu0306. Mineral abbreviations according to Kretz (1983). (b) Na element map of typical muscovite–paragonite association in the matrix of Al-rich metapelite sample APi0301. (c) Photomicrograph of graphite-bearing metapelite ALu0603 showing porphyroblasts of garnet and staurolite overgrowing the schistosity. Staurolite is highlighted by a white rim. The graphite-free vein (arrow 1) consists essentially of white micas and pre-dates both staurolite (arrow 2) and garnet (arrow 3). (d) Back-scattered electron (BSE) image of fine association of paragonite, biotite and chlorite in the matrix of APi0601 with plagioclase overgrowing the matrix. (e) Photomicrograph of a polished section of AMo0410 with Bt-rich and Grt-rich layers. Garnet cores are rich in spessartine and thus lighter in colour (see inset). (f) X-ray map showing zoning in X_{Na} in muscovite related to paragonite breakdown (metapelite AMo0410).

Mineral separation and X-ray diffraction

In most samples used for ^{40}Ar–^{39}Ar dating, two grain sizes were separated. Samples were manually crushed in a steel mortar, and then sieved. Fraction size was selected according to the average grain size observed in thin section: a fine fraction of 50–150 µm (termed Ms100 or Bt100) and a coarser one of 150–250 µm (Ms200 or Bt200). These sieved fractions correspond to the true crystallographically continuous grain size (Table 1). Size fractions >250 µm present difficulties, owing to the abundance of impurities or to thin interlayers of muscovite and paragonite. A vibrating table was used to enrich the mica fraction, and a Frantz® magnetic separator to separate biotite from white micas. Muscovite being Fe-richer than paragonite, the use of a

Table 1: Natural size of optically continuous mica crystals in thin section (in μm)

Sample	Muscovite		Paragonite		Margarite		Biotite	
	Length	Thickness	Length	Thickness	Length	Thickness	Length	Thickness
ALu0306	30–120	10–20			50–150*	<5–20	100–1000	30–700
ALu0601	50–250	10–100						
ALu0603	200–500	50–100	100*	10–30				
API0301	100–200	10–100	100–200	10–100				
API0601			50–100*	5–20			100–400	20–50
API0603	100–250	50–100	20–100*	1–10			200–1000	100–500
AMo0409	500–800	60–100					200–3000	50–300
AMo0410	50–400	20–100	50–100	5–10			500–2000	200–500

*Typically form clusters or bands up to 0·5–1·0 mm in size.

strong magnetic field helped in some cases to separate these white micas. After sieving, mechanical and magnetic separation, mineral separates were cleaned in an ultrasonic bath with deionized water for a few minutes, then with acetone. A prolonged ultrasonic bath (15–30 min) disaggregated mica sheets, but impurities (quartz, chlorite, graphite) tended to stick to the micas. Where this happened, a second sieving was necessary to eliminate the smaller flakes. Because of the presence of micrometre-sized interlayers of muscovite and paragonite or biotite and chlorite, the use of a smaller grain-size fraction allowed a more complete mechanical and visual (handpicking) separation of muscovite from paragonite or of biotite from chlorite, as interlayers tended to break apart and became easier to identify under a binocular microscope. Final handpicking under a binocular microscope ensured visually pure fractions. In ALu0306 and API0601, white micas were difficult to separate from quartz and chlorite, even after repeated attempts by gravimetric and magnetic techniques. Three samples (API0301, ALu0601, -03) contained exceedingly small amounts of biotite, hence no satisfactory separates for ^{40}Ar–^{39}Ar dating could be obtained. The presence of graphite represented an analytical problem: analyses of low-grade graphite-rich rocks from the Apennines (I. M. Villa, unpublished data, 1990) have shown that hydrocarbon interference, especially on mass 36, can predominate over Ar from the sample. Therefore, it was decided to concentrate the separation efforts on graphite-poor rocks and to carefully handpick graphite-free micas.

The purity of mineral separates was checked by X-ray diffraction (XRD) on a Panalytical X'Pert-Pro X-ray diffractometer at the Institut für Geologie, Universität Bern. This instrument is equipped with a Cu-anode tube set to operate at 40 kV and 40 mA and to cover the 2θ range from 4° to 40°. To enhance [001] reflections, mica separates were sedimented with acetone on a glass slide. The intensity ratios of muscovite [006] and paragonite [003] peaks were used to estimate the mode of paragonite–muscovite mixtures (Frey, 1977). This technique allows identification of impurities as low as 0·5%. In the margarite-bearing sample ALu0306, peak ratios could not be accurately calculated owing to weak muscovite peaks and the presence of quartz. For biotite separates, a qualitative intensity ratio of chlorite [004] and biotite [006] peaks was used to estimate the proportion of chlorite.

^{40}Ar–^{39}Ar stepwise heating

The analytical procedure is described in the Appendix. For each run, K, Cl and Ca concentrations were calculated from the total ^{39}Ar, ^{38}Ar and ^{37}Ar, respectively. In the present study, these totals were used to recalculate the percentage of impurities in the mineral separate. For this, a mass-balance calculation is applied assuming (1) the K and Ca concentrations stem only from biotite or muscovite and paragonite (or margarite) and (2) K- and Ca-free impurities identified by XRD can be present (e.g. quartz, chlorite or kyanite). The assumption that impurities contain no K and Ca may be an oversimplification in the rare cases where finely intergrown chlorite gained ^{37}Ar and ^{39}Ar by recoil during irradiation. When XRD did not reveal the existence of a third phase in the mineral separate, the modal abundances of muscovite and paragonite were calculated based exclusively on total K from the Ar measurement.

In the pioneering days, age spectra were considered to be valid only if they were flat (so-called 'plateau'; e.g. Dalrymple & Lanphere, 1974). In our mineral separates, the presence of at least two white-mica generations is common. Disentangling a mixture requires using common-denominator three-isotope correlation diagrams,

such as, for example, the $^{37}Ar/^{39}Ar$ and $^{38}Ar/^{39}Ar$ ratios, which are equivalent to the Ca/K and Cl/K ratios, respectively. This class of diagrams allows the recognition of binary (or ternary; Villa, 2001*l*) mixtures and a characterization of the phase releasing the argon. Thus, stepwise heating results have been demonstrated to yield a significant age, even in the absence of a plateau, because of the possibility of identifying the different Ar reservoirs in a sample (e.g. Villa *et al.*, 1996, 2000; Belluso *et al.*, 2000; Di Vincenzo & Palmeri, 2001). Microprobe analysis of all studied samples shows that $Ca/K_{margarite} \gg Ca/K_{paragonite} > Ca/K_{muscovite} \approx Ca/K_{biotite}$ and $Cl/K_{biotite} > Cl/K_{muscovite}$.

Cl/K ratios in paragonite and margarite could not be determined precisely, as Cl concentrations were below or near the detection limit of the electron microprobe (50–120 ppm). A mixture of muscovite with paragonite or margarite should essentially yield a variation in $^{37}Ar/^{39}Ar$ and, to a lesser extent, in $^{38}Ar/^{39}Ar$. A reliable identification is possible either if one or more steps have similar Ca/K ratios (as determined from the $^{37}Ar/^{39}Ar$ ratios) compared with the Ca/K ratios measured by EMP analysis of the phase to be dated (Villa *et al.*, 1996) or, if a linear correlation is observed, by extrapolating the line to the EMP value of the Ca/K or Cl/K ratio (Villa *et al.*, 2000). However, this technique is limited by the EMP detection limit of Ca in muscovite and paragonite or of K in margarite, and of Cl in any white mica studied. Moreover, Ca/K and/or Cl/K variations may be observed exclusively if the Ar release temperatures of each phase constituting the separate are different. The degassing behaviours of muscovite, phengite, Fe- or Mg-rich biotite are sufficiently different to allow discrimination in most cases (e.g. Zimmermann, 1970; Wijbrans & McDougall, 1986). The degassing of margarite and paragonite compared with muscovite requires further investigation; this is discussed in the Appendix.

The final age assignment was constrained by the average of 'isochemical' steps characteristic of one mineral phase. The selection of isochemical steps is based on the fact that they yield similar $^{37}Ar/^{39}Ar$ and $^{38}Ar/^{39}Ar$ signatures (i.e. Ca/K and Cl/K), characteristic of the analysed phase (Krumrei *et al.*, 2006; Hetherington & Villa, 2007). These two ratios must be (1) well resolved from background (i.e. sample mass must be sufficiently large; Müller *et al.*, 2002), and (2) coherent with the independently known value for each phase obtained, for instance by EMP. In contrast, when steps yield variable Ca/K or Cl/K ratios, they are considered as 'heterochemical' steps. If so, an age for each component of the mineral separate may be obtained either by identifying the isochemical steps yielding the Ca/K and Cl/K of the phase to be dated or by deciphering the trend in a Ca/K or Cl/K vs age correlation diagram, and extrapolating this trend to the known value of each mineral to be dated.

MINERAL COMPOSITIONS

Mineral assemblages and mineral compositions were found to be very similar from sample to sample. This is not surprising as the six metapelite samples represent a fairly uniform metamorphic grade and rock type. A set of averaged analyses is given in Supplementary Data Table 1, where the bulk-rock composition of all samples is also seen to be similar. Only the two metamarls ALu0304 and ALu0306 are richer in CaO, but poorer in Al_2O_3. Moreover, ALu0306 has the highest MgO content (5·5%) of all the studied samples. In our sample suite, two white micas commonly coexist, but the occurrence and abundance of muscovite and paragonite or margarite depend on the P–T conditions and on the bulk-rock Ca, Na and K concentrations (Supplementary Data Table 1).

In all but one sample, muscovite is devoid of systematic chemical zoning. Analyses across each thin section are slightly heterogeneous typically within ±0·03 in X_K [= K/(Ca + Na + K); Fig. 3a]. The K concentrations of muscovite are highest in the absence of paragonite and in the presence of margarite ($X_K > 0·89$; Supplementary Data Table 1), whereas X_K may decrease to 0·75 in muscovite coexisting with paragonite. In parallel with the increase in metamorphic grade from Lucomagno Pass to Molare, an increase of the Na concentration in muscovite is observed (Fig. 3a). In sample AMo04*l*0, muscovite rims locally are significantly more sodic where surrounded by paragonite [0·3 vs 0·2 in $X_{Na} = Na/(Ca + Na + K)$; Fig. 2f]. The phengite component in muscovite is low in all studied samples [Fe 0·05–0·16, Mg 0·08–0·12 and Si 3·06–3·17 atoms per formula unit (a.p.f.u.)].

Margarite is exclusively found in metamarls. It shows a solid solution towards paragonite, with up to 0·30 X_{Na} (Franz, 1977), but only a minor muscovite component (<0·02 X_K; Fig. 3a). In sample ALu0306, more heterogeneity up to ±0·1 X_{Ca} [= Ca/(Ca + Na + K)] is observed compared with muscovite, but neither back-scattered electron (BSE) images nor element mapping could reveal compositional variation in flakes. Most of this variation occurs from flake to flake (Fig. 2a). The presence of chlorite interlayers is probably responsible for the decrease in Ca, Na and Al content correlated with the increase in Si, Fe and Mg content. At Molare, margarite included in garnet yields slightly higher Na concentrations, but only traces of K.

Paragonite compositions are homogeneous in each grain and over the thin section, with $X_{Na} \approx 0·83$ at Lucomagno and Piora and up to 0·87 at Molare (Fig. 3a, Supplementary Data Table 2). Comparing muscovite and paragonite in two metapelites, the Ca and K concentrations of paragonite are anti-correlated, ranging from $X_{Ca} \approx 0·10$ and $X_K \approx 0·07$ (in API030*l*) to $X_{Ca} \approx 0·03$ and $X_K \approx 0·11$ (in AMo04*l*0). This reflects an increase in metamorphic grade. The larger spread in paragonite composition from AMo04*l*0 is

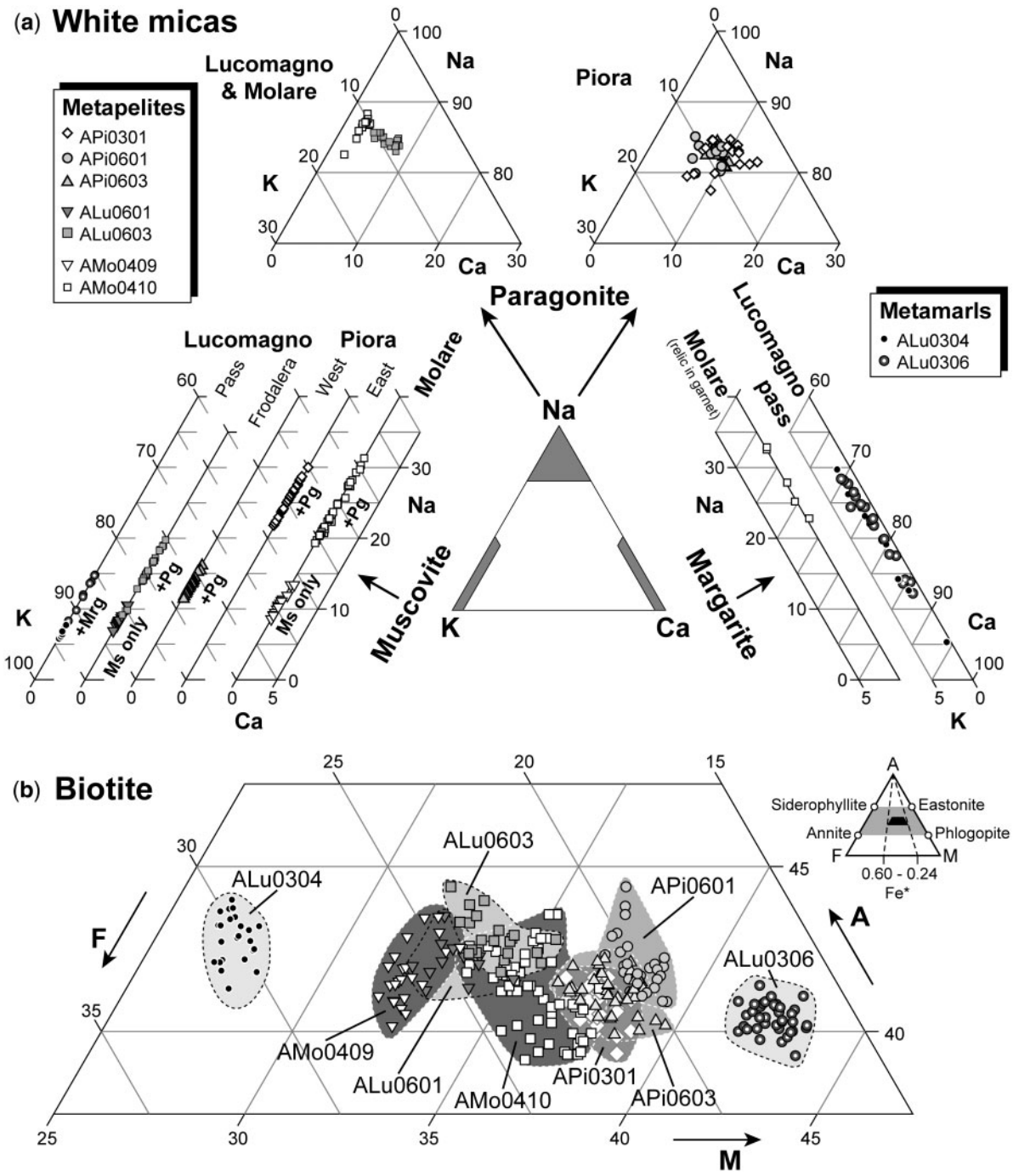

Fig. 3. Mica compositions. (a) Ternary Ca–Na–K diagram for margarite (right), paragonite (top) and muscovite (left). (b) Ternary Al–Fe–Mg (AFM) diagram for biotite.

mostly related to fine intergrowths of paragonite with larger muscovite crystals (K-richer analysis; Fig. 3a).

Biotite grains are internally homogeneous in composition, but variations are observed from grain to grain at millimetre to centimetre scale, and may reach ±0·03 in Fe* [= $Fe_{total}/(Fe_{total} + Mg)$]. A even larger variation is observed in AMo0410, probably related to garnet- or biotite-rich layers of different rock composition (Fig. 2e). The sample analysed comes from a Grt-rich zone, with some metamorphic segregation around the numerous small, strongly zoned garnet crystals (Fig. 4a). In samples from a similar metamorphic grade, a range of Fe* in

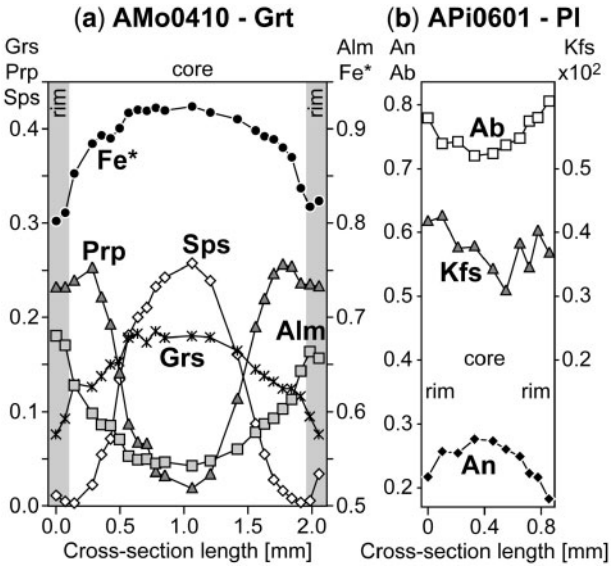

Fig. 4. (a) Typical garnet cross-section in a metapelite from Molare (AMo0410). A slight increase in Mn content at the rim is indicative of resorption (grey band). However, Fe* remains constant or slightly higher, suggesting that this occurred near the thermal maximum or at slightly lower *T*. (b) Exceptional zoning in plagioclase related to the partial paragonite decomposition in a metapelite from Piora (APi0601) showing an anorthite-richer core. An, Ab or Kfs = Ca, Na or K/(Ca + Na + K).

biotite is observed, from 0·40–0·45 in an Fe-rich metapelite at Lucomagno, to 0·33–0·38 at Piora and to 0·28–0·30 in Mg-rich metamarl ALu0306 (Fig. 3b).

Chloritization of biotite is usually minor and local, but it is observed in all of the studied samples. It is easily identified in BSE images, and slightly lower K concentrations measured by EMP indicate the presence of chlorite lamellae in biotite in each sample. Where textures suggest that chlorite resulted from the retrogression of biotite, the Fe* ratio of both phases is very similar. In chlorite from ALu0306 and APi0601 Fe* is lower than in coexisting biotite. This partitioning attests to prograde growth of chlorite in these two samples and reflects chemical equilibrium with biotite at or near the thermal peak.

Garnet is almandine-rich with typical prograde zoning patterns showing a regular decrease in Fe*, almandine and spessartine components, accompanied by an increase in the pyrope component (Fig. 4a). Grossular contents generally decrease from core to rim, except in the kyanite-free sample APi0301.

Plagioclase is typically homogeneous in composition (oligoclase to andesine). In sample APi0603, two grains yield slightly variable composition (An_{24} and An_{29}; Supplementary Data Table 1). A clear zonation is visible in APi0601 and in APi0301, where An contents decrease from core to rim (Fig. 4b), and correlate with the progressive breakdown first of epidote, followed by paragonite.

Staurolite is present in a majority of the selected metapelites; it is homogeneous in composition. From sample to sample, the Fe* ratio is slightly variable according to the bulk-rock composition (from 0·74 to 0·83; Supplementary Data Table 1). Local equilibrium in non-communicating compositional domains can also affect its composition (e.g. ALu0603, ALu0601: higher Fe* for grains in contact with garnet, but lower for grains in the matrix; Supplementary Data Table 1).

P–T CONDITIONS

Thermobarometry was applied using the software 'TWQ' (Berman, 1991). The thermodynamic database 'JUN92.dat' (Berman, 1988, 1991) was augmented by the staurolite model defined by Nagel *et al.* (2002). Phase equilibria were calculated in the system SiO_2–Al_2O_3–TiO_2–FeO–MgO–CaO–Na_2O–K_2O–H_2O. For use in thermobarometry, coexisting minerals were analysed in millimetre-sized domains, commonly around a garnet porphyroblast, but avoiding direct contact. Our study indicates that this strategy minimizes apparent disequilibrium effects related to local variations in bulk composition (Allaz, 2008).

Metamorphic equilibration was last achieved under lower amphibolite-facies conditions. The stable mineral assemblage is typically made up of biotite and one or two white micas (muscovite with paragonite or margarite), together with plagioclase, garnet and commonly kyanite or staurolite. Table 2 gives the equilibrium assemblage and *P–T* results calculated. A small but significant increase of *P–T* conditions is revealed, from 0·65 GPa and 540–560°C at Lucomagno Pass to 0·8–0·9 GPa and 580–600°C at Molare. In most cases, a close intersection of all the computed equilibria for each sample (e.g. Fig. 5a) was found, indicating that chemical equilibrium between the rock-forming minerals was approached, and rather well preserved, with only minor effects of retrogression. Only samples APi0301 and AMo0410 show a larger spread of the equilibria, suggesting some disequilibrium (Fig. 5c). Systematic exclusion analysis (Table 2) suggests that biotite may be out of equilibrium in AMo0410, as calculations omitting this mineral yield lower *P–T* conditions and a tighter intersection of equilibria. Moreover, biotite is more chloritized (although still only slightly) in this sample, and garnet shows an Mn-richer rim indicating minor resorption (Fig. 4a). A second average based on four well-calibrated equilibria (Fig. 5b and d, Table 2; 'Best eq.', see file 'rxtns_calib.dat' available with TWQ 2.32 package), yield slightly lower *P–T* conditions for samples APi0301 and AMo0410, which further suggests a slight disequilibrium.

P–T conditions calculated for the specific mineral assemblages in this study largely hinge on Fe–Mg equilibria involving garnet, staurolite, and biotite, all of which essentially depend on *T*. White-mica and, to a lesser extent,

Table 2: Thermobarometric results from TWQ in metapelite and marly samples from the three selected areas

Sample	LIR	All equilibria			Best eq.		Solid solutions							Pure		Not in *PT*		Graphite
		P (kbar)	*T* (°C)	$X(H_2O)$	*P*	*T*	Ms	Pg	Mrg	Bt	Grt	St	Pl	Ky	Qtz	Ilm	Rt	*T* (°C)
ALu0304	5	6·2 ± 0·2	566 ± 8	0·98	6·3	573	X		X	X	X		X		X	X		551 ± 13
ALu0601	6	7·3 ± 0·6	546 ± 22	0·27	7·5	562	X			X	X	X	X	X	X	±	X	
No biotite	4	7·5 ± 0·3	555 ± 12	0·29			X			o	X	X	X	X	X	±	X	
ALu0603	8	8·8 ± 0·6	577 ± 23	0·36	8·9	580	X	X		X	X	X	X	X	X	±	X	
No biotite	6	8·7 ± 0·5	569 ± 19	0·34			X	X		o	X	X	X	X	X	±	X	
No paragonite	6	9·0 ± 0·6	583 ± 20	0·36			X	o		X	X	X	X	X	X	±	X	
APi0301	7	8·3 ± 0·8	570 ± 28	0·46	7·3	511	X	X		X	X	X	X		X	X		
No biotite	5	8·5 ± 0·5	585 ± 14	0·55			X	X		o	X	X	X		X	X		
No paragonite	5	8·3 ± 0·9	573 ± 20	0·50			X	o		X	X	X	X		X	X		
APi0601	4	9·0 ± 0·5	585 ± 16	0·41	8·9	579		X		X	X		X	X	X	X		
APi0603	8	8·9 ± 0·7	579 ± 24	0·39	8·8	572	X	X		X	X	X	X	X	X		X	587 ± 9
No biotite	6	8·5 ± 0·6	561 ± 23	0·33			X	X		o	X	X	X	X	X		X	(SPi0306)
No paragonite	6	8·9 ± 0·7	576 ± 27	0·33			X	o		X	X	X	X	X	X		X	
AMo0409	5	6·6 ± 0·2	573 ± 11	0·60			X			X	X	X	X		X	X		
AMo0410	7	8·4 ± 0·5	594 ± 14	0·47	8·4	569	X	X		X	X	X	X	X	X	X	±	
No biotite	5	7·8 ± 0·6	563 ± 20	0·47			X	X		o	X	X	X	X	X	X	±	
No paragonite	5	8·3 ± 0·5	587 ± 21	0·40			X	o		X	X	X	X	X	X	X	±	
AMo0504	3	7·1	586	0·33			X			X	X		X		X	X		604 ± 7

Uncertainties are exclusively based on the spread of the intersection points between calculated equilibria; this does not include the analytical uncertainty of the mineral analyses or the errors in the thermodynamic models. The average *P–T* conditions in columns on the left are based on the observed mineral assemblage (columns on the right) and include all computed equilibria. For some samples, biotite or paragonite was excluded from the calculation to check for its equilibrium state (exclusion analysis). The 'Best eq.' *P–T* average is based exclusively on a set of well-calibrated equilibria [see file 'rxtns_calib.dat' available with TWQ 2.32 package]. LIR, number of linearly independent reactions.
X, phase included in calculation. o, phase excluded from calculation.

plagioclase compositions typically play a minor role in the *P–T* calculation, and small changes in activity do not result in large *P–T* offsets. Errors on the *P–T* calculation given in Table 2 are exclusively based on the spread of the intersections of all computed mineral reactions. Temperature is extremely well constrained (±20°C), whereas the pressure determination is typically subject to larger uncertainties (±0·07 GPa).

In a few graphite-rich samples, we applied the geothermometer based on the degree of organization of carbonaceous material (Table 2; Beyssac *et al.*, 2002). Results confirm the *T* obtained by TWQ thermobarometry, with a maximum of 551 ± 13°C at Lucomagno pass (sample ALu0304), 587 ± 9°C at Piora (sample SPi0306 near APi0601 and APi0603) and 604 ± 7°C at Molare (sample AMo0504).

In addition to TWQ thermobarometry, the evolution of mineral assemblages in each sample was investigated with THERIAK-DOMINO (de Capitani & Petrakakis, 2010) over the range of *P–T–X*(H_2O) conditions needed to model the chemical and modal evolution of micas. In general, the *P–T* fields of stability at unit water activity yield results in line with the observed mineral assemblages and *P–T* calculations from TWQ (e.g. ALu0603; Fig. 6). Applied to the metamarl ALu0306, the presence of margarite requires that the molar fraction of water in these samples also remained high [$X(H_2O) \approx 1·0$–$0·7$]. At $X(H_2O) = 0·8$, the *P–T* range of this reaction is situated between 0·4 GPa, 450°C and 0·8 GPa, 580°C. This is in line with the *P–T* conditions calculated from the neighbouring sample ALu0304 (Table 2). These results are taken as further evidence for preservation of equilibrium *P–T* conditions in all samples.

^{40}Ar–^{39}Ar DATING

^{40}Ar–^{39}Ar age data from each mineral separate are discussed from samples of lower (Lucomagno pass) to higher metamorphic grade (Molare). First, we present results for

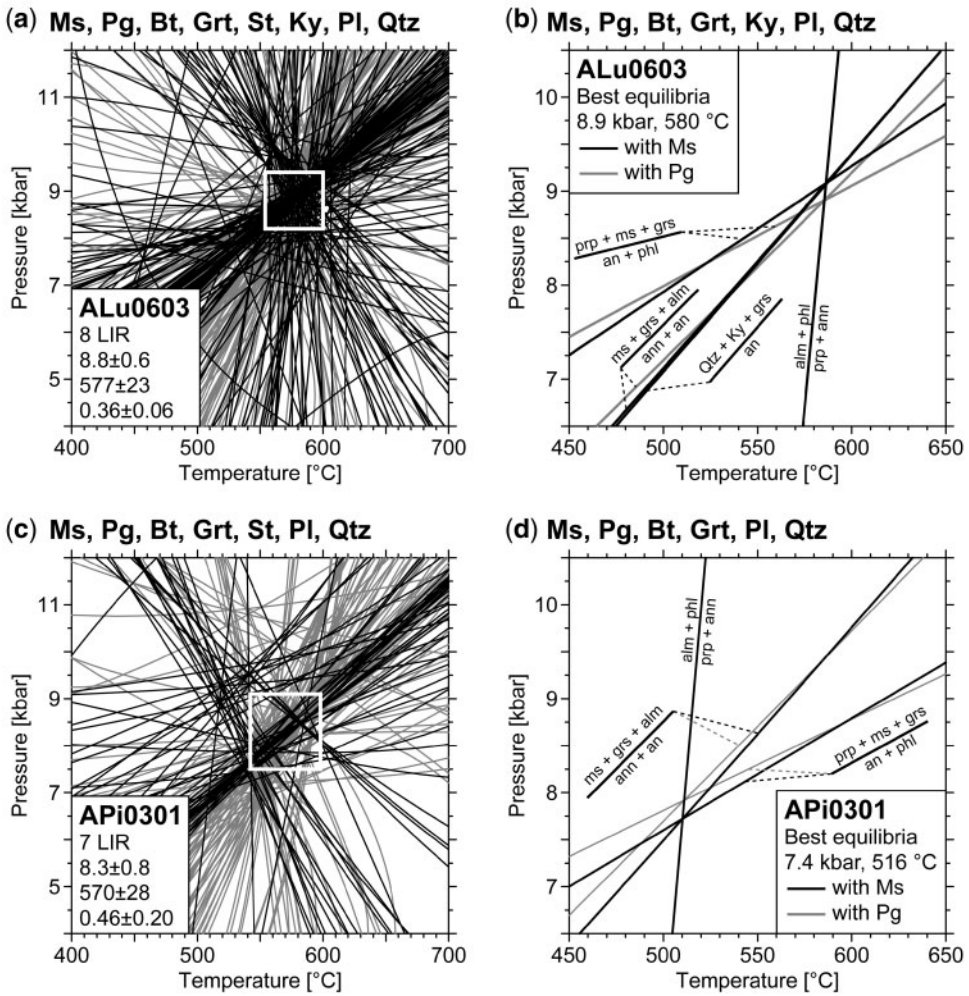

Fig. 5. *P–T* calculation results using TWQ for (a, b) a typical Al-rich metapelite from Frodalera (ALu0603), and (c, d) from Piora (APi0301). (a, c) Complete set of equilibria calculated; mineral assemblage given above each *P–T* diagram. Black curves are fluid-conserved equilibria; grey curves are dehydration equilibria. White open square indicates the average *P–T* conditions. Mineral compositions used for calculation, identification and listing of all equilibria are available on request from J.A. (b, d) A set of three (four) well-calibrated equilibria from TWQ results confirms that garnet, micas, plagioclase (and kyanite) are fully equilibrated [see file 'rxtns.calib.dat' available with TWQ 2.32 package].

white mica, and then for biotite. Results are summarized in Table 3 and the complete set of analyses is given in Supplementary Data Table 2. Most ages from Table 3 were determined from steps yielding a plateau in the age spectrum and typically correspond to isochemical steps in monomineralic separates. For mineral separates composed of two white micas, the analysis of *in vacuo* Ar release from micas and mica mixtures (see Supplementary Electronic Material) shows that muscovite, paragonite and margarite release their Ar at different furnace T (Supplementary Data Fig. 1). This means that each step is a variable mixture of gas from the micas in the sample, which results in a variation of the Ca/K ratio between each step (heterochemical steps). To determine the 'true' age of muscovite, paragonite or margarite, we extrapolate the age towards the Ca/K value determined by EMP for each white mica composing the mineral separate (Table 4).

White micas

XRD results from the first white-mica separate of the metamarl ALu0306 reveal <1–2% muscovite with >95% of margarite and some quartz ('Mrg-rich'; Table 3), whereas the second separate contains <10% muscovite ('Mrg ± Ms'; Table 3). From ^{40}Ar–^{39}Ar analyses, we deduce the contribution of muscovite to the total ^{39}Ar release to be 43·1% and 89·1%, respectively (Table 3). ^{40}Ar–^{39}Ar results are similar for both separates, but their Ca/K and Cl/K ratios differ (Fig. 7, Supplementary Data Table 2). Both samples apparently record the same stage of evolution, with plateau ages at 17·6 ± 1·4 and

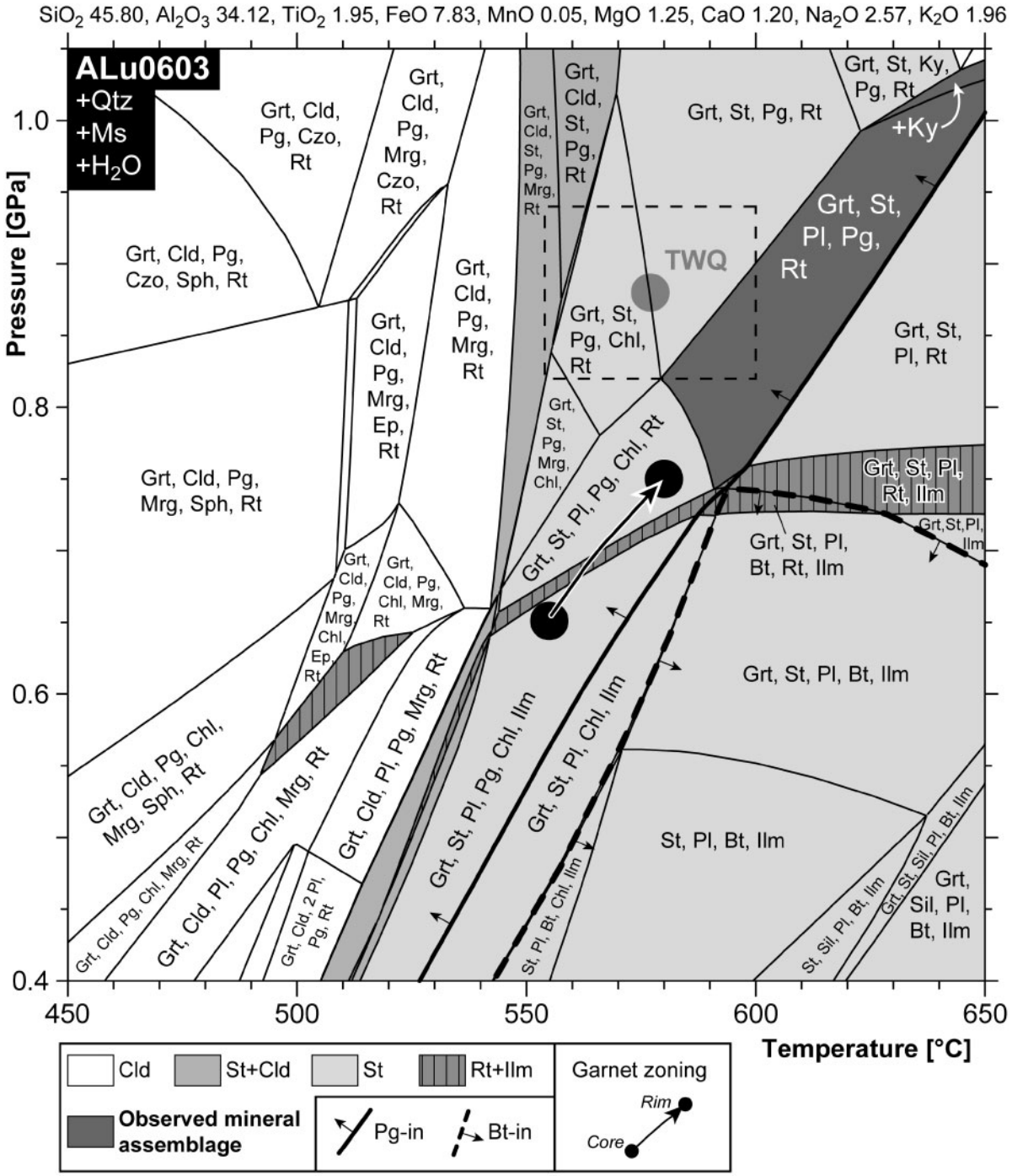

Fig. 6. Stability fields of mineral assemblages in metapelite ALu0603 computed with THERIAK-DOMINO near water-saturated condition [$X(H_2O) > 0{\cdot}99$] for the bulk-rock composition given above the diagram. Quartz and muscovite are stable over the entire P–T window. The grey circle indicates the TWQ calculation result; the dashed rectangle denotes the uncertainty. Chemical zoning in garnet reveals a prograde growth history from 555°C, 0·65 GPa to 580°C, 0·75 GPa.

18·04 ± 0·78 Ma for Mrg-rich and Mrg ± Ms, respectively (Table 3). Ca/K is lowest in Mrg ± Ms (0·8–13), and demonstrates that Ar release is dominated by muscovite (Fig. 7b). In the Mrg-rich separate, the steps yield Ca/K values from 4·4 (step 4) to 66·9 (step 5; Fig. 7b); that is, higher than for the Mrg ± Ms separate. When results are combined, a weak negative correlation in Ca/K vs age is visible. However, extrapolation to the EMP value

Table 3: Summary of mineral separates and ^{40}Ar–^{39}Ar dating results

Mineral separates[1]				XRD results[2]		^{40}Ar–^{39}Ar ages and total K, Ca, and Cl[3]							Mass balance[4]			
Sample	Separate	Mesh (μm)	Weight (mg)	Mineral and impurities	Peak ratio	Steps	Status	^{39}Ar (%)	Age (Ma) error 95% c.l.	Totals K (%)	Totals Ca (%)	Totals Cl (ppm)	% Ms[5]	% Mrg or Pg[5]	% Ca-, K-free phase	%^{39}Ar from Ms
White mica																
ALu0306	Mrg-rich	125–250	13·9	Mrg, Qtz, ±Ms	–	3–10	P	76·0	17·6 ± 1·4	0·22	5·89	5·7	1·1	81·1	17·8	43·1
	Mrg ± Ms	125–250	29·7	Mrg, Qtz, Ms	–	3–6	P	97·2	18·04 ± 0·78	0·85	4·33	9·6	9·0	59·7	31·3	89·1
ALu0601	Ms100	50–150	14·36	Pure Ms	100	3–8	P, I	90·7	16·30 ± 0·23	7·20	0·14	54·1	86·3	–	13·7?	–
	Ms200	150–250	12·10	Pure Ms	100	3–7	P, I	93·9	16·66 ± 0·20	>5·44	>0·17	>28·6	>65·1	–	<34·9?	–
ALu0603	Ms100	50–150	11·93	Ms, ±Pg	98·8	3–10	P, I	95·6	16·36 ± 0·22	6·27	0·16	47·9	83·7	16·3	–	97·9
	Ms200	150–250	20·57	Pg, Ms, Qtz	13·6	1–6	P	99·9	16·67 ± 0·39	1·47	0·32	184·6	14·9	46·1	39·0	74·4
APi0301	Ms + Pg	150–250	14·1	Ms, Pg, ±Qtz	47·6	4–14	P (±)	89·6	16·87 ± 0·35	3·07	0·58	18·0	37·3	50·5	12·3	87·0
APi0601	Ms100	50–150	11·55	Pg, Qtz, Ms, ±Chl	~20[6]	2	1 step	45·8	15·18 ± 0·70	0·81	0·06	104·4	9·9	8·4	81·7	91·2
	Ms200	150–250	13·75	Pg, Qtz, ±Ms, ±Chl	~5[6]	2	1 step	49·2	16·42 ± 0·88	0·51	0·33	158·8	1·4	47·4	51·2	20·7
APi0603	Ms-A	50–150	16·07	Ms, ±Pg	93·9	4–10	P, I	88·9	15·88 ± 0·15	6·52	0·21	75·1	85·7	14·3	–	98·3
	Ms-B	50–150	16·97	Ms, Pg	70·9	4–9	P, I	81·0	15·48 ± 0·19	5·25	0·31	47·7	66·7	33·3	–	95·0
	Ms-C	150–250	15·18	Ms, Pg, ±Qtz	79·4	3–9	P, I	91·2	15·73 ± 0·19	5·14	0·26	47·9	65·5	31·5	3·0	95·2
	Ms-D	150–250	20·57	Pg, Qtz, ±Ms	4·3	3–7	P (±)	81·8	15·0 ± 2·1	0·96	0·66	84·2	4·2	81·2	14·6	33·1
						6–7	I	31·1	15·7 ± 1·3							
AMo0409	Ms	200–250	18·3	Pure Ms	100	6–10	P, I	86·3	17·85 ± 0·61	6·30	0·28	21·7	72·8	–	27·2?	100·0
AMo0410	Ms ± Pg	200–250	16·6	Ms ± Pg, ±Ky, ±Qtz	96·7	4, 6, 7	I Ms	42·6	18·35 ± 0·59	3·62	1·21	82·6	<47·3	<52·7	–	94·9
						5, 8–11	I Ms + Pg	31·1	16·87 ± 0·60							
Biotite													% Bt	% Chl		
ALu0306	Bt	125–200	6·4	Bt, Chl	2·1	3–8	P (±)	80·0	17·65 ± 0·33	6·65	0·86	541·9	80·7	19·3		
						3, 8	I	41·1	17·61 ± 0·38							
APi0601	Bt100	50–150	11·46	Bt, ±Chl	1·0	3–7	P, I	77·5	14·85 ± 0·21	6·41	0·13	147·6	83·8	16·2		
	Bt200	150–250	11·08	Bt, ±Chl	0·8	3–9	P, I	92·8	14·84 ± 0·23	5·94	0·34	569·9	77·7	22·3		
APi0603	Bt100	50–150	9·12	Bt, Chl	2·6	3–8	P	94·6	14·72 ± 0·26	6·04	0·46	355·1	80·3	19·7		
	Bt200	150–250	12·08	Bt, Chl	2·1	4, 6–8	P, I	58·0	15·29 ± 0·25	6·48	0·18	483·9	86·1	13·9		
AMo0409	Bt	50–125	17·3	Bt, ±Chl	<0·5	3–9	P, I	93·8	16·25 ± 0·81	6·65	0·40	44·6	83·2	16·8		
AMo0410	Bt	50–125	16·6	Bt, Chl	2·6	5, 13	I	42·3	16·37 ± 0·40	6·18	1·09	165·4	83·8	16·2		

[1]Minerals prepared for ^{40}Ar–^{39}Ar dating with names of sample and mica separate, weight and grain-size fraction.
[2]Presence of impurity detected by XRD and muscovite–paragonite or chlorite–biotite peak intensity ratios. XRD peak intensity ratio calculated as follows: $100 \times Ms[006]/(Ms[006] + Pg[006])$ and $100 \times Chl[004]/(Chl[004] + Bt[006])$. The peak ratio for white micas is semi-quantitative (Frey, 1977), whereas chlorite and biotite ratios are only qualitative.
[3]Summary of ^{40}Ar–^{39}Ar ages. First column lists the steps used for average age and is followed by the status of selected steps: P, 'plateau' age; I, 'isochemical' steps (constant Ca/K and Cl/K), matching with EMP data or extrapolated to measured compositions. Errors are given at the 95% confidence level. Total K, Cl and Ca concentrations were calculated from the total measured ^{39}Ar, ^{38}Ar and ^{37}Ar. Low totals may reflect both admixture of Ca-, K-free phase(s) and variable absolute mass spectrometer sensitivity; they do not imply deviations from stoichiometry, which is controlled by EMP.
[4]Mass-balance calculation for the mica generations contained in each separate, based on pure end-member K and Ca concentrations obtained by EMP and on total K and Ca concentrations calculated from artificial Ar isotopes.
[5]If more than three phases are present, as in the two white-mica separates of APi0601, this ratio is a maximum value.
[6]Because of strong interference of quartz [101] on muscovite peak [006], a qualitative ratio based on Ms [002] and Pg [002] is considered.

Table 4: Summary of ^{40}Ar–^{39}Ar ages obtained by extrapolations from Ca/K age diagrams for paragonite and margarite

Sample		Age (Ma) from extrapolation	At Ca/K	MSWD/probability	Age difference (Ma)
ALu0306	Ms	18·04 ± 0·80	0·00	0·28/0·99	1·0 ± 2·0
	Mrg	17·1 ± 2·5	65 ± 11		
ALu0603*	Ms	16·34 ± 0·23	0·00	0·31/0·98	−0·1 ± 0·3
	Pg	16·43 ± 0·20	0·84 ± 0·11		
APi0301	Ms	17·18 ± 0·76	0·00	0·21/0·99	2·3 ± 5·7
	Pg	14·9 ± 5·6	1·58 ± 0·28		
APi0603	Ms	15·79 ± 0·11	0·00	1·14/0·27	2·0 ± 1·3
	Pg	13·81 ± 1·30	1·02 ± 0·08		
AMo0410	Ms	18·93 ± 0·83	0·00	1·3/0·23	5·6 ± 2·4

Column 'At Ca/K' indicates the EMP value assumed in the regression.
*Excluding step 5 of Ms200.

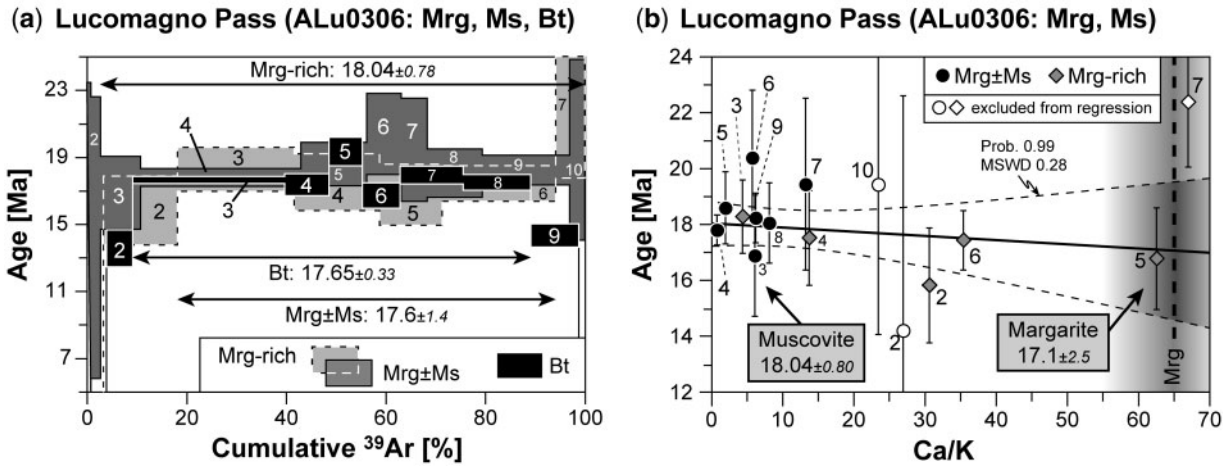

Fig. 7. Ar isotope results from margarite-rich metamarl at Lucomagno Pass (ALu0306). (a) Age spectra for biotite and two white-mica separates. In this figure, as in subsequent age spectra, errors are 1σ, whereas average ages are 2σ. (b) Ca/K vs age correlation diagram. Error envelope is given as 2σ. First and last steps were excluded from the regression (white diamonds and circles). The existence of a spread as a function of step *T* is evidence that muscovite and margarite have different *in vacuo* breakdown temperatures (see Supplementary Data Fig. 1).

for the Ca/K ratio of margarite, 65, yields statistically indistinguishable ages (Fig. 7b, Table 4).

At Frodalera, both white-mica separates in ALu0601 are pure muscovite (Table 3). They show homogeneous and low Ca/K, Cl/K ratios for the major steps 3–8 for Ms100 and steps 3–7 for Ms200 (Fig. 8c). These steps yield isochemical (and plateau) ages of 16·30 ± 0·23 and 16·66 ± 0·20 Ma, respectively. In ALu0603, muscovite and paragonite were enriched in two fractions by selecting different grain sizes (Table 3). Thus, the Ca/K ratio for these separates shows significant variations (Fig. 8c), especially in the paragonite-rich separate Ms200 (0·15–0·85). Despite these differences in Ca/K ratio, ^{40}Ar–^{39}Ar dating of the separates from ALu0603 yields very similar results as for ALu0601: 16·67 ± 0·39 Ma for the coarse fraction (150–250 μm) and 16·36 ± 0·22 Ma for the fine one (50–150 μm; Fig. 8a and b, Table 3). No correlation between age and Ca/K is observed, and extrapolation to the EMP value for the Ca/K ratio of muscovite or paragonite yields identical results. Both micas thus record the same age (Table 4).

XRD results for APi0301 indicate a 50:50 mixture of muscovite and paragonite in the white-mica separate. It yields an apparent age plateau at 16·87 ± 0·35 Ma (Fig. 9a, Table 3). However, steps are clearly heterochemical; that is, they yield variable Ca/K and Cl/K ratios (Fig. 9b). The isochemical age from low-Ca/K steps is 17·04 ± 0·62 Ma

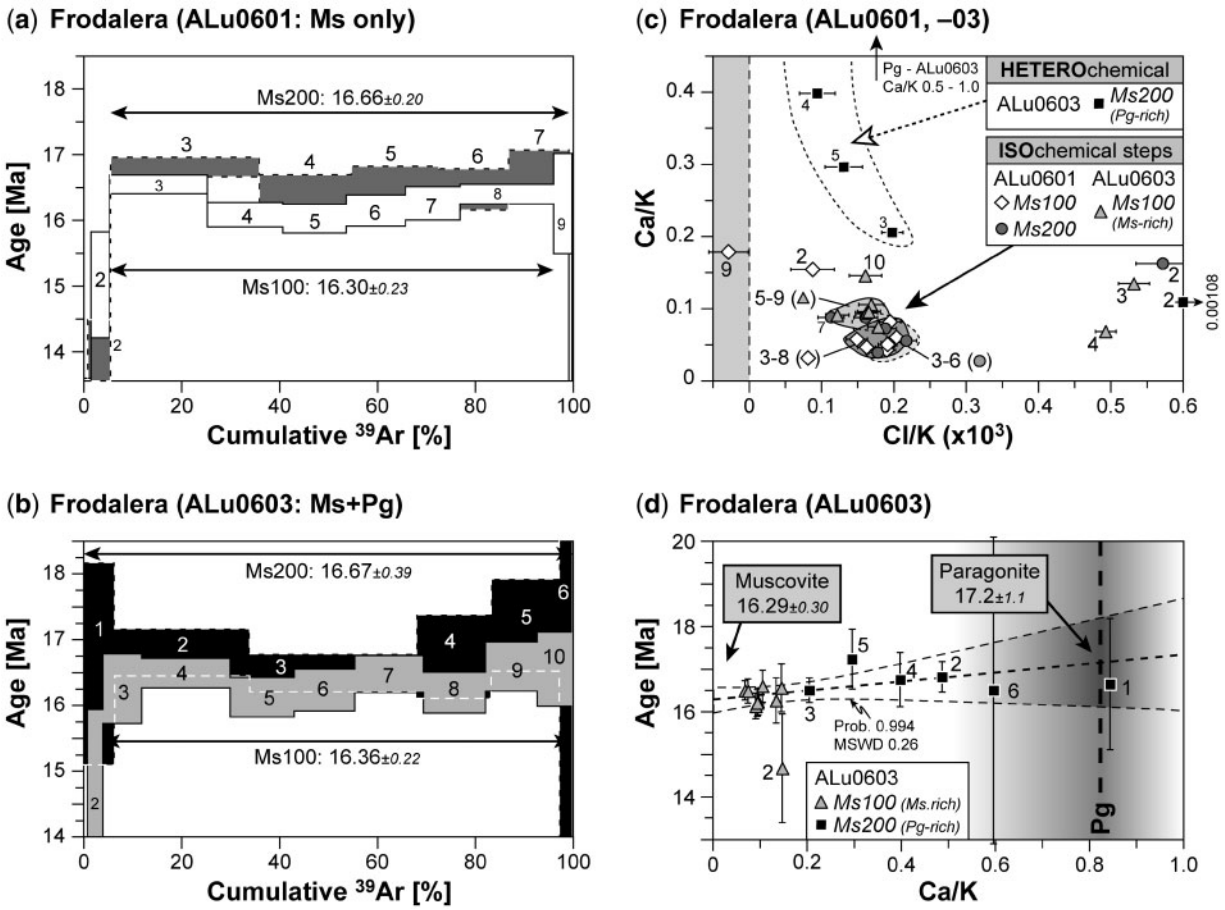

Fig. 8. (a, b) Ar isotope results from two Al-rich metapelites from Frodalera. (a) Age spectra for coarse- and fine-grained muscovite ALu0601 and (b) muscovite-rich (Ms100) and paragonite-rich (Ms200) separates from ALu0603. (c) Ca/K and Cl/K correlation for mica separates of ALu0601 and ALu0603. All three muscovites have very similar chemical signatures (grey fields) and only the paragonite-rich fraction Ms200 of ALu0603 (black square) has higher Ca/K ratios. (d) Ca/K vs age correlation diagram. Error envelope is given as 2σ.

(steps 7–12), whereas steps with Ca/K around 0·3 yield 16·68 ± 0·59 Ma (steps 4 and 5; Fig. 9). In a Ca/K vs age correlation diagram, a negative correlation is observed. Extrapolating to the paragonite Ca/K ratio yields a statistically unresolved and imprecise age (14·9 ± 5·6 Ma; Table 4). However, the trend observed in other samples (see below) suggests that paragonite might be younger than muscovite in this sample.

Muscovite and paragonite from sample APi0603 are enriched in two fractions. Nearly pure muscovite constitutes the finest and more magnetic fraction (Ms-A; 50–150 μm), whereas paragonite dominates the coarser and less magnetic one (Ms-D; 150–250 μm; Table 3). Two intermediate white-mica separates contain *c.* 70 and 80% muscovite (Ms-B: fine and less magnetic; Ms-C: coarse and more magnetic; Table 3). The ^{39}Ar release in Ms-A, Ms-B, and Ms-C is dominated by muscovite, whereas paragonite dominates in Ms-D (Pg-rich; Table 3). All age results of the four white-mica separates are similar, three of them being statistically indistinguishable. Of the two finer fractions, Ms-A (15·88 ± 0·15 Ma) and Ms-B (15·48 ± 0·19 Ma), the latter shows a small but significant difference (Table 3, Supplementary Data Table 2). The two coarser fractions (Ms-C and Ms-D) give isochemical ages of 15·73 ± 0·19 and 15·7 ± 1·3 Ma (Table 3, Supplementary Data Table 2). A weak dependence of age on Ca/K is observed, and an age extrapolation toward the EMP value of paragonite yields 13·8 ± 1·3 Ma (Table 4).

Step ages from the paragonite-rich separates of APi0601 have large errors owing to the low K concentration in paragonite. In both separates, step 2 concentrates more than 40% of the total ^{39}Ar release and yields ages of 15·18 ± 1·40 Ma (Ms100) and 16·42 ± 1·76 Ma (Ms200; Supplementary Data Table 2). Step 3 of Ms100 yields the lowest Ca/K and 16·64 ± 1·21 Ma.

White-mica separates from AMo0409 are pure muscovite, and isochemical steps yield 17·85 ± 0·61 Ma (Table 3, Fig. 10a). Consistent with petrographic observation, the

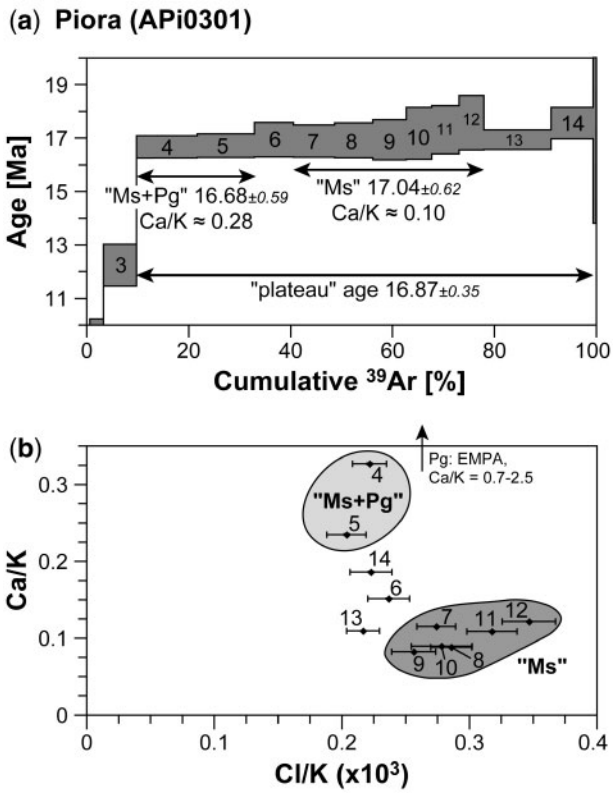

Fig. 9. (a) Age spectra for white-mica separate in the muscovite- and paragonite-bearing metapelite APi0301. (b) The Ca/K vs Cl/K correlation diagram shows two distinct fields: steps 4 and 5 are identified as partly affected by the signature of paragonite (whose measured Ca/K ratio lies outside the plot frame and is indicated by an arrow); steps 7–12 yield lower Ca/K and higher Cl/K, and are related to muscovite degassing.

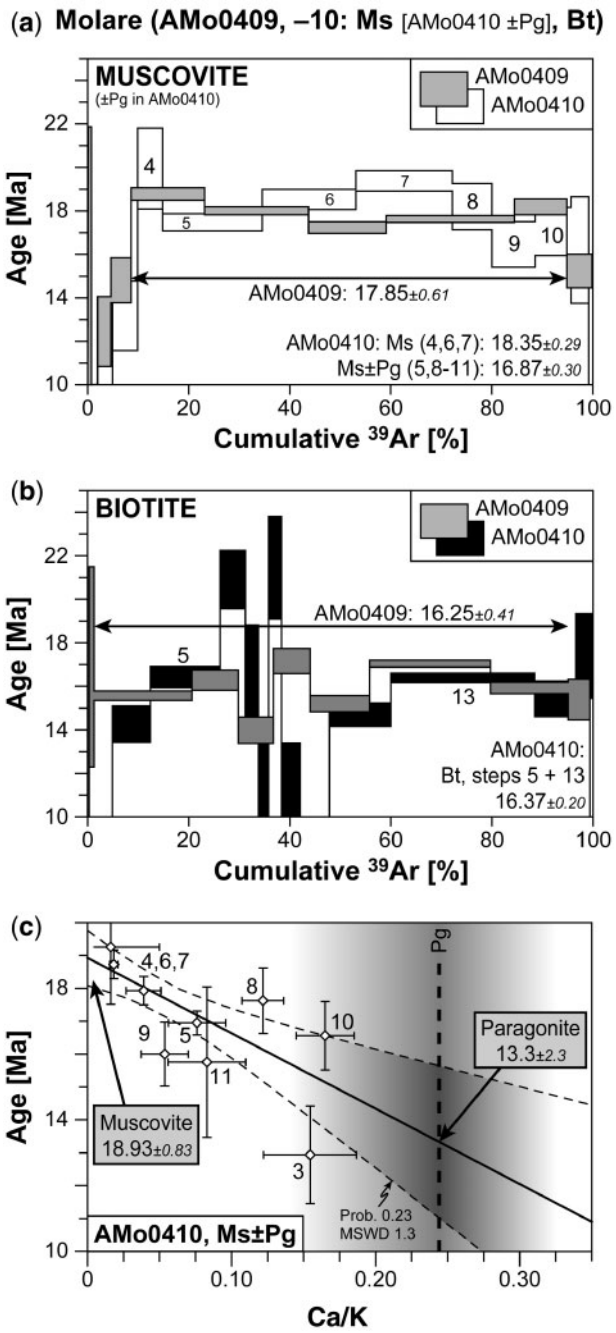

Fig. 10. Ar isotope results from Molare. (a) Age spectra for muscovite and (b) biotite from AMo0409 and AMo0410. (c) Ca/K vs age correlation diagram in muscovite–paragonite mixture AMo0410. Extrapolation toward the Ca/K value in paragonite directly determined by EMP (grey field, 0·25 ± 0·09) yields the age of the pure paragonite. Error envelope is given as 2σ.

white-mica separate from AMo0410 contains a minimum of 4% paragonite and traces of quartz and kyanite (Table 3). This separate yields an apparently older age, reaching 18·35 ± 0·59 Ma in steps 4, 6 and 7 having the lowest Ca/K, whereas steps 5 and 8–11 give an age of 16·87 ± 0·60 Ma and have higher Ca/K (Table 3, Fig. 10a and c). A negative correlation between age and Ca/K ratio is most probably related to minor paragonite. Extrapolation toward the composition of paragonite yields 13·3 ± 2·3 Ma (Fig. 10c, Table 4).

Biotite

The biotite separate from Lucomagno Pass yields a plateau age at 17·65 ± 0·33 Ma and a similar isochemical age of 17·61 ±0·38 Ma based on steps 3 and 8 having the lowest Ca/K and Cl/K (Fig. 7a, Supplementary Data Table 2). It is also the oldest age among all the biotite separates (Table 3). This sample is the only one yielding nearly identical ages of biotite and white micas. In all other samples, our ^{40}Ar–^{39}Ar data indicate that biotite is systematically younger than muscovite.

In APi0601 and -03, coarse fractions yield an isochemical age at low Ca/K and Cl/K (Supplementary Data

Table 2) of 14·84 ± 0·23 and 15·31 ± 0·20 Ma, respectively, whereas fine fractions yield 14·85 ± 0·21 and 14·72 ± 0·26 Ma. In separate Bt100 of sample APi0603, steps are heterochemical with two clusters in a Ca/K–Cl/K correlation diagram. The anti-correlation between Fe* and Cl concentration obtained by EMP analysis of different biotite grains suggests that two chemically distinct generations exist, with higher Cl (700–1800 ppm vs < 200 ppm) and lower Fe* concentrations (0·345 vs 0·370). However, no age difference is recorded for these chemically different biotites, and we infer a co-genetic growth of these different biotite populations (Cl-rich, steps 3–5 at 14·71 ± 0·49 Ma; Cl-poor, steps 6–8, at 14·74 ± 0·30 Ma; Supplementary Data Table 2).

The biotite separate from AMo0409 yields 16·25 ± 0·81 Ma, with homogeneous and low Cl/K and Ca/K (Fig. 10b, Supplementary Data Table 2). In AMo0410, Ar release from biotite yields a highly discordant spectrum (Fig. 10b), which we attribute to the high chlorite content in the separate (Table 3; see discussion below). Ca/K and Cl/K vary significantly, but no correlation exists with the age variation. Steps 5 and 13 have the lowest Ca/K and low Cl/K ratios (~0·0078 and ~0·0016, respectively), and correspond to the two major ^{39}Ar release peaks (Supplementary Electronic Material). Thus, they probably reflect degassing of biotite *sensu stricto*. They yield an isochemical age of 16·37 ± 0·40 Ma, in agreement with the biotite age from neighbouring sample AMo0409.

DISCUSSION

Most samples from this study show well-preserved equilibrium conditions. Metamorphic grade increases slightly from Lucomagno pass (540–560°C, 0·5–0·7 GPa) to Molare (580–600°C, 0·7–0·9 GPa), in good agreement with previous studies (Engi *et al.*, 1995; Todd & Engi, 1997).

The assemblage muscovite–paragonite–plagioclase remained stable throughout the post-peak evolution in samples from Frodalera–Lucomagno, but not from Piora and Molare. In the samples from the former area, retrogression appears to be subordinate, such as in sample ALu0603, and accordingly ages for muscovite and paragonite are indistinguishable (Tables 3 and 4). The highest-grade sample AMo0410 from Molare shows the largest discrepancy by having the highest age difference between muscovite and paragonite or biotite. Samples APi0601 and APi0603 from Piora are intermediate both in terms of their age gap and of the duration of the passage through the paragonite-out field. The age difference between paragonite and muscovite increases with metamorphic grade, from Lucomagno (–0·09 ± 0·30 Ma) to Piora (2·0 ± 1·3 Ma) and to Molare (5·6 ± 2·4 Ma; Table 4). The age difference between biotite and muscovite also increases from north to south, but less so than between muscovite and paragonite. The lowest grade sample analysed at Lucomagno Pass yields indistinguishable ages for muscovite and biotite, whereas at Piora the muscovite age (APi0603; Table 4) is 0·50 ± 0·27 to 1·07 ± 0·28 Ma older than those for biotite Bt200 and Bt100, respectively (Table 3). In samples from the Molare area, muscovite and biotite differ by 1·6 ± 0·9 Ma in AMo0409 and 2·3 ± 0·9 Ma in AMo0410.

A similar age pattern between muscovite and paragonite is predicted from first principles (Dahl, 1996), owing to their similar crystal structure. This raises the question as to why there is an age difference observed in samples from higher grade at Piora and Molare. Diffusion theory requires that the bulk material, in this case the mica, remained stable (Giletti, 1974), which is no longer the case where and when a metamorphic reaction occurred; our detailed petrological investigation shows that sample AMo0410 and, to a lesser extent, APi0301 were subjected to subtle disequilibrium with stronger paragonite resorption owing to plagioclase growth, and also more pronounced chloritization of biotite. Interpreting paragonite ages as being related to a cooling age might be an oversimplification. It is more likely that the retrograde consumption of paragonite to form plagioclase is responsible for the age discrepancy between paragonite and muscovite ages. The role of such a reaction in controlling the isotopic record has been repeatedly discussed (Chopin & Maluski, 1980; Wijbrans & McDougall, 1986; Villa, 1998*b*, 2004; Di Vincenzo *et al.*, 2004; Gouzu *et al.*, 2006; Glodny *et al.*, 2008*a*, 2008*b*). In the next section, mica stability is investigated in some key samples; then the role of mineral reaction in the Ar retention properties is discussed and compared with the effects of thermal resetting (diffusion).

The constraints provided by the comparison of grain sizes are partly ambiguous. An age difference between two different grain-size fractions of the same mineral is expected for purely diffusive Ar loss. For an activation energy of 200 kJ mol^{-1} and a cooling rate equal to the long-term average cooling rate of our samples, 30°C Ma^{-1}, doubling the grain size increases the Dodson (1973) closure temperature by about 20°C, which translates to a predicted age difference of *c.* 0·7 Ma. Our data show a marginally significant age dependence on grain size for muscovite APi0601 and biotite APi0603, and no significant difference for muscovite ALu0601 and biotite APi0601 (Table 3). In particular, for sample APi0601 we have analysed four mica fractions: the muscovite behaves consistently with thermally activated Ar loss, and the coexisting biotite does not. One could speculate that the biotite was affected by subtle retrogression reactions (below we will argue that this often occurs). The absence of a significant age difference in muscovite ALu0601 is not understood. In general, the issue remains unresolved and would require further investigation under very strictly controlled petrological characterizations.

Mica stability in Al-rich pelites

Paragonite and margarite react to form plagioclase at conditions near the calculated peak P and T for samples from Lucomagno Pass. These white micas can be completely consumed at higher T or lower P via a dehydration net transfer reaction such as

$$\mathrm{Pg(or\ Mrg) + Qtz \rightarrow Ab(or\ An) + Ky + H_2O.} \quad (1)$$

The close association of kyanite, plagioclase and paragonite in samples APi0601, APi0603, and AMo0410 lends support to this type of reaction. However, kyanite is not found in margarite-bearing samples. Computed P–T and T–$X(CO_2)$ relations suggest that a higher Tschermak component in chlorite and biotite accommodates the Al release from margarite breakdown (Allaz, 2008). In metapelites, staurolite can be produced when chlorite or biotite are added as reactants (e.g. ALu0603; Fig. 6). The first plagioclase is not pure albite but oligoclase ($An_{20–30}$) in any of the studied Ca-poor metapelites. The Ca component most probably comes from the former coexistence of paragonite and margarite at greenschist-facies conditions (Frey, 1969; Livi *et al.*, 1997) or the presence of carbonate in metamarls (e.g. ALu0306, ALu0304) or epidote in the slightly calcic metapelites.

We investigate the evolution of tri- and di-octahedral micas on the basis of P–T grids modelled for sample ALu0603 (Fig. 6). Figure 11a presents a simplified petrogenetic grid for this sample restricted to the plagioclase-in, paragonite-out, muscovite-out, K-feldspar-in and chlorite-in reactions at unit water activity. An Al-poorer metapelite is also considered for comparison (AMo0410; Fig. 11b). Modelled phase equilibria predict that muscovite remains stable, whereas paragonite is partially consumed and replaced by plagioclase. Within an interval of *c.* 50°C, paragonite, plagioclase, and muscovite re-equilibrate continuously through $Na_{-1}Si_{-1}CaAl$ or $Na_{-1}K$ exchange reactions. Muscovite experiences only minor chemical and modal changes in the investigated P–T range, resulting in slight muscovite overgrowth owing to paragonite decomposition and/or minor resorption during staurolite growth (Fig. 11c and d).

From petrographic observation and thermobarometric investigation (Figs 5a, b and 11c, e), paragonite is stable in samples from Lucomagno. However, paragonite from Molare is close to its stability limit and was largely consumed by plagioclase formation. This is inferred from the low modal amount, the fine flake size (commonly <50 μm; Figs 2f and 11f), and the computed P–T model (compare Fig. 11c and d). White mica and plagioclase compositions predicted by THERIAK during paragonite decomposition have lower X_K for muscovite and higher X_{An} for plagioclase, but similar X_{Na} for paragonite (Fig. 11c and d). These variations are similar to those measured by EMP (Fig. 3a). Such a variation in composition is observed in sample AMo0410 with a Na-richer rim in muscovite and slightly An-richer rim in plagioclase (0·135 vs 0·166 X_{An}; Fig. 2f; Supplementary Data Table 1).

Biotite can also be affected by chloritization along this retrograde path. Indeed, below 0·75 GPa, chlorite is again stable below 590–540°C (Figs 6 and 11a, b). P–T data determined for the samples investigated are close to the chlorite-in reaction (e.g. Fig. 11a and b), such that minor chloritization was likely to occur upon cooling where aqueous fluid became available. The slight disequilibrium observed with TWQ results in sample AMo0410, as also in APi0301, suggests that both paragonite breakdown and chloritization of biotite reactions occur during early decompression or retrogression.

Concerning margarite, only one sample was investigated (ALu0306). The large modal amount of margarite (*c.* 10–20%; Fig. 2a), the stability of both biotite and chlorite, and the computed P–T stability field of plagioclase–margarite point to an equilibrium of these minerals in this specific sample from Lucomagno pass.

Mineral reaction, retrogression

We argue that late re-equilibration is noticeable in the Molare area, less so in Piora and negligible in Lucomagno. Retrogression is likely to have been most pronounced shortly after the thermal peak at ≤0·7 GPa, where the kinetics of reaction were favourable. As 'dry' environments are more likely to have preserved metastable parageneses (e.g. Bjørnerud *et al.*, 2002), we suggest that retrogression was linked to fluid percolation during exhumation (e.g. chloritization) or to a dehydration reaction occurring during decompression, in our case the paragonite breakdown. The different equilibrium P–T conditions calculated in samples from a restricted area reflect parts of their P–T paths around T_{max} (Fig. 11a and b). However, the mineral assemblage reflects the driest P–T condition rather than T_{max} (Proyer, 2003). Thus, contouring H_2O isopleths may reveal the most likely point of last equilibration.

Assuming these models are correct, equilibrium was reached when the P–T path became tangent to these isopleths. Applied to our system, H_2O isopleths are parallel to the paragonite-out or chlorite-in reactions (Fig. 11g and h). Our calculations predict final equilibrium within the paragonite stability field for samples from Lucomagno and Piora, whereas final equilibrium for samples from Molare most probably occurred after paragonite breakdown. Concerning biotite, we demonstrated that the chlorite stability field is crossed shortly after the peak of metamorphism: chloritization of biotite is obvious in some samples, especially in AMo0410.

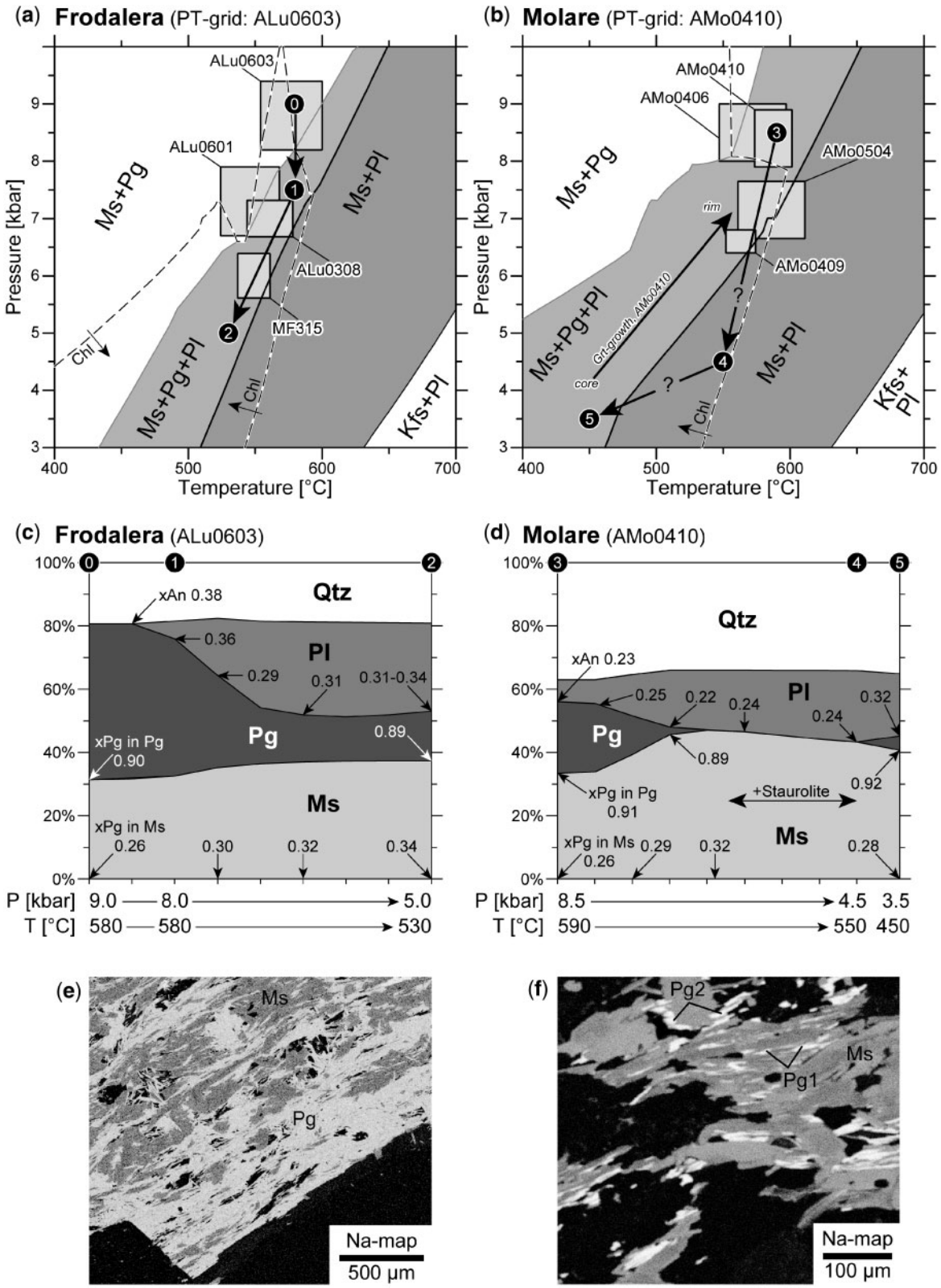

Fig. 11. (a, b) Stability of muscovite, paragonite, plagioclase and K-feldspar (a) in Al-rich (ALu0603) and (b) Al-poorer metapelite (AMo0410). Grey rectangles are *P–T* calculation results from TWQ relevant to each area (Frodalera and Molare). (c, d) Modal evolution of muscovite, paragonite, plagioclase and quartz along the retrograde *P–T* paths shown in (a) and (b). Numbers are mineral isopleths: mole fraction of sodic endmember in paragonite or muscovite and anorthite contents in plagioclase. (e, f) Na element map in thin section (e) from ALu0603, where paragonite is at equilibrium with muscovite), and (f) from Molare (AMo0410). In the latter, paragonite appears as tiny flakes interlayered with muscovite. Pg1 denotes primary paragonite, whereas Pg2 probably represents the secondary paragonite appearing during retrogression. (g, h) H_2O contents (wt %) in the mineral assemblage for samples (g) ALu0603 and (h) AMo0410 as a function of *P–T*.

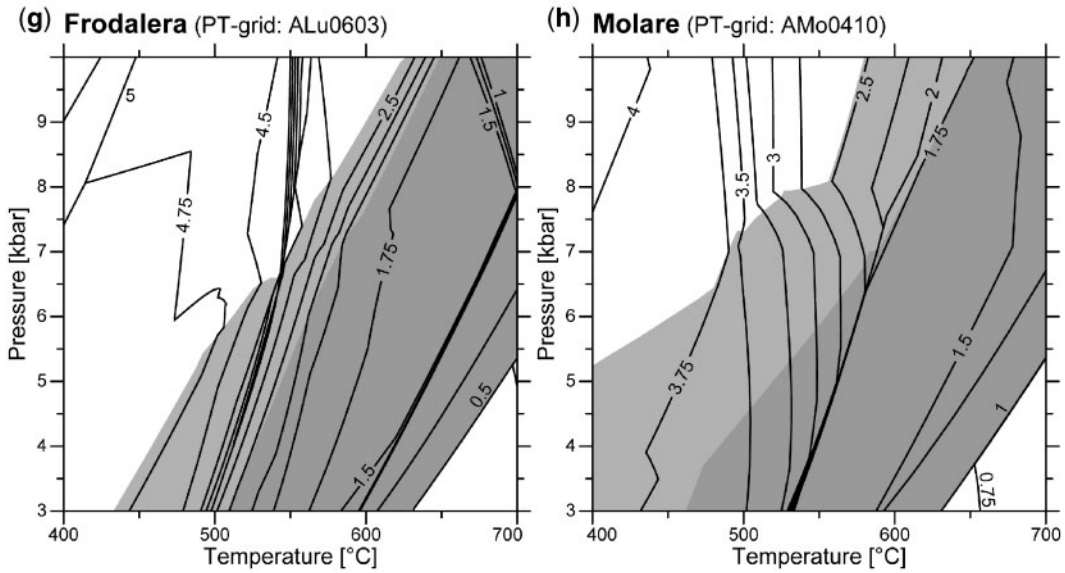

Fig. 11. Continued.

Does Ar retention record cooling or (re-)crystallization?

To be significant, an isotopic age needs to be related with certainty to a geological process. The Mesozoic metasediments discussed here are affected by a single orogenic cycle during the Alpine orogeny. Thus, resetting of the Ar record in micas cannot be affected by inheritance of pre-metamorphic relics and must be related either to crystallization, to diffusion ('cooling age'), or to re-equilibration along the retrograde path.

Ar diffusion in micas is usually considered for interpreting K–Ar ages from rocks equilibrating at $T > 500^{\circ}$C. Jäger *et al.* (1967) and Purdy & Jäger (1976) originally estimated K–Ar closure T of micas at 350°C for muscovite and 300°C for biotite. However, these values and inferences are not undisputed: (1) the peak metamorphic T was underestimated (Villa & Puxeddu, 1994), as was the persistence of pre-Alpine inheritance in polymetamorphic minerals (Hammerschmidt & Frank, 1991, fig. 2; Villa, 1998*b*, fig. 1); (2) these studies did not take into account the fact that diffusion will be overwhelmed by retrograde net-transfer reactions where these take place (e.g. Chopin & Maluski, 1980; Di Vincenzo *et al.*, 2004; Glodny *et al.*, 2008*a*, 2008*b*), notably metamorphic reactions involving fluids along the retrograde path. Regarding laboratory determination of Ar loss, it has been argued (Villa, 2010) that hydrothermal experiments are flawed owing to dissolution–reprecipitation reactions and phase destabilization. The only two publicly available muscovite data sources (Hess *et al.*, 1987; Harrison *et al.*, 2009) report ample evidence of both, which means that the derived Ar loss rates refer to multiple processes and represent strict upper limits for true volume diffusion. This fact leaves field-based assessments of muscovite retentivity as by far the most reliable estimates. The closure temperature for Ar loss proposed here, 520–540°C, is in perfect agreement with those inferred on the basis of complete elimination of pre-metamorphic inheritance (Hammerschmidt & Frank, 1991; Villa, 1998*b*, 2006; Di Vincenzo *et al.*, 2004).

Partial recrystallization and/or exchange reactions (possibly fluid-enhanced) along the retrograde path induce chemical re-equilibration and chemical resetting of both paragonite and biotite. Whenever this occurred, the metamorphic reaction rather than mere volume diffusion controlled the resetting of the Ar clock. The muscovite–paragonite age gap gives important insights into the relation between petrology and isotopic record. The repeated observation that muscovite ages are greater than or equal to, but never lower than paragonite ages implies that the process leading to the age gap occurred at a T when muscovite was already closed to Ar diffusive losses (i.e. $T < 540^{\circ}$C). We argue that the cause of the age gap is the consumption of paragonite at the paragonite-out boundary and its renewed crystallization when the rock re-entered the paragonite stability field. We therefore propose that paragonite ages are younger in highest-grade rocks because they were more completely consumed and thus more accurately record the timing of the reaction forming a second generation of retrograde paragonite after plagioclase. Thermodynamics predicts the composition of primary or secondary paragonite to be very similar ($X_{Na} = 0{\cdot}89$–$0{\cdot}91$ vs $0{\cdot}92$; Fig. 11f), thus rendering the identification of renewed crystallization difficult. Texturally, however, paragonite in sample AMo0410 is present as

micrometre-size interlayers within muscovite (Pg1) and also as larger paragonite flakes surrounding muscovite (Pg2; Fig. 11f). The latter type is viewed as the secondary paragonite, whereas the former represents some remnant of the primary paragonite. Moreover, Na-richer muscovite rims occur locally, and we interpret them as overgrowths related to paragonite breakdown. Compared with the cores, rims consisting of Na-richer muscovite should yield a younger age, and this may further explain the scatter in the age spectrum and in the age vs Ca/K correlation diagram (Fig. 10a and c): subordinate young Na-rich muscovite rims coexist with the older and more abundant Na-poor muscovite, whereas young paragonite (Pg2) coexists with minor older paragonite (Pg1). Compared with Pg1 and muscovite (core and rim), Pg2 yields the youngest age related to its recrystallization along the retrogression, as suggested by the ^{40}Ar–^{39}Ar ages (Fig. 10c).

The purely diffusive Ar retention of biotite is more difficult to assess, because biotite commonly shows non-negligible petrological disequilibrium when investigated in sufficient detail using systematic exclusion analysis (e.g. AMo0410; Table 2). Petrographic observation, thermobarometry, and mineral analysis indicate the omnipresence of stable primary chlorite in Mg-rich samples; Fe-richer biotite is likely to have been slightly chloritized during retrogression, especially in samples from Molare. Where biotite reacted to form staurolite or chlorite during decompression or cooling (e.g. Nagel *et al.*, 2002), its Ar isotopic record would have been (partially) reset. Where biotite and chlorite reached complete re-equilibration of both major-element contents and isotope composition, biotite may date the chloritization event, otherwise the biotite age will lie anywhere between the two events. In addition, chloritization is well known to result in ^{39}Ar recoil artefacts (e.g. Di Vincenzo *et al.*, 2003, and references therein): ^{39}Ar may move from one mineral phase to a contiguous one and be degassed at a different oven T from the degassing of ^{40}Ar, creating a 'disturbed' age spectrum. The same can happen to ^{37}Ar and ^{38}Ar produced during neutron irradiation of Ca and Cl, respectively. A diagnostic feature is that the odd isotopes $^{37}Ar_{Ca}$ and $^{39}Ar_{K}$ have recoil distances that are orders of magnitude larger than those of the even isotopes (i.e. the artificial $^{38}Ar_{Cl}$ and the radiogenic $^{40}Ar^{*}$; Onstott *et al.*, 1995; Villa, 1998*a*). This makes it straightforward to identify a recoil artefact by using three-isotope correlation diagrams having $^{39}Ar_{K}$ as the common denominator and $^{40}Ar^{*}$, ^{37}Ar or ^{38}Ar as numerators (see, e.g. Villa & Buettner, 2009; their age vs Cl/K diagram in Fig. 7b). The finer grain size of secondary chlorite may have produced recoil artefacts (Di Vincenzo *et al.*, 2003). This effect might be responsible for the strongly disturbed age spectrum observed in the biotite separate from sample AMo0410. However, such correlation trends are weak in biotite AMo0410, and the increasing Ca/K ratio in all of the steps, except for steps 5 and 13, appears to rule out major recoil artefacts.

The diagnostic pattern of a recoil artefact is not observed in any of the other mica separates, which consist of large and essentially pristine flakes. A more precise quantification of this effect would require a transmission electron microscopy study (e.g. Kogure & Banfield, 2000; Di Vincenzo *et al.*, 2003) to investigate the possible interlayering of muscovite and paragonite. The latter effect has been documented to occur at lower grade (Livi *et al.*, 1997), but such a fine-grained muscovite–paragonite association is apparently no longer present in the amphibolite facies, when white micas coarsen to form distinct and large grains (e.g. Fig. 2b).

Biotite ages are indistinguishable from muscovite ages at Lucomagno Pass, and younger in higher-grade rocks. We expect the latter result on the basis of the predictions by Dahl (1996). The biotite–muscovite age coincidence is an unexpected observation. In principle, two chronometers give the same age (1) when both record complete retention of radiogenic daughters, or (2) when both record incomplete retention of radiogenic daughters but the 'cooling rate' was extremely fast, or (3) simply by coincidence. As the general context of our samples supports a high spatial regularity, the third explanation can be discarded. In the absence of isotopic inheritance, it is the oldest ages in a given field area that most closely approach the purely diffusive behaviour. We therefore focus on the biotite–muscovite pair in sample ALu0306 to deduce that Mg-rich biotite has a very similar Ar diffusivity to muscovite [albeit slightly lower, as predicted by Dahl (1996)]. Again, this agrees with the independent estimates based both on a re-examination of the original Giletti (1974) data (Villa, 2010) and on the Larderello metamorphic and plutonic biotite (Villa & Puxeddu, 1994; Villa *et al.*, 2006): namely, that muscovite and biotite retain Ar completely below *c.* 520–540°C and 450–500°C, respectively (Allaz, 2008). Even higher closure temperatures were proposed for micas in dry metamorphic environments (Balogh & Dunkl, 2005).

It is also useful to view our samples in the broader context of additional geochronological data from similar rocks in the same area. In samples equivalent to APi0601 and ALu0603, monazite was dated at 18–19 Ma by U–Pb (Janots *et al.*, 2008, 2009). Because Alpine monazite in this sample grew near the thermal peak, its age records the time when T was at 570–580°C. Muscovite, being slightly younger, records a slightly later point along the P–T path estimated to be 520–540°C (Allaz, 2008). It is important to stress that Ar diffusion is the fastest process only in the absence of chemical retrogression and fluid-assisted recrystallization, and only in these cases is the concept of 'closure temperature' legitimate. This condition is fairly exceptional and needs to be demonstrated on a sample-by-sample

basis by detailed petrological tests. Such tests are critical points for any geochronological investigation, as prograde and retrograde metamorphic reactions alike induce not only a re-equilibration of major elements, but also the resetting of isotopic systems.

CONCLUSIONS

By combining petrological and geochronological data on mica-bearing Mesozoic metasediments of the northern part of the Central Alps, it is possible to document cases of well-preserved phase equilibria, partial disequilibrium, and retrograde re-equilibration. The information required for these distinctions comes from observations in thin sections combined with precise thermobarometric calculations and theoretical phase relations. In the area studied, calculated peak metamorphic conditions vary between $560 \pm 20^{\circ}C$, $0{\cdot}62 \pm 0{\cdot}02$ GPa at Lucomagno Pass and $590 \pm 20^{\circ}C$, $0{\cdot}84 \pm 0{\cdot}05$ GPa at Molare.

Many of the samples analysed here contain finely intergrown mixtures of two white micas (i.e. muscovite with paragonite or margarite). XRD analysis and stoichiometry of micas recalculated from the ^{40}Ar–^{39}Ar data were necessary quality controls for the analysed separates. By using diagrams correlating mica composition and age, we were able to estimate ages for each white mica making up the mineral separates. Muscovite invariably gave the oldest ages; biotite and paragonite gave ages that were in some cases indistinguishable from muscovite, in others significantly younger than the latter, but there is no simple, regular pattern of muscovite–biotite–paragonite age relations. We argue that it is the retrogression history of each sample, not the regional T field, that has the decisive control on the isotopic record.

We observe that recrystallization or fluid-assisted processes will overrun diffusion whenever they occur. Such retrograde processes are not easily related to a specific P–T interval upon cooling, as their limiting factor is the availability and composition of (hydrous) fluid. Thermobarometry may help in identifying and quantifying the P–T conditions in which secondary minerals grew. Upon cooling and decompression, samples along typical P–T paths generally encounter one of the reactions delimiting the stability of biotite, paragonite, or margarite. In the sample suite studied, these limits were crossed above 500°C, where reaction progress is likely to have effected local retrogression of these micas. Petrographic evidence for this can be subtle, but is common at grain scale (e.g. local chlorite specks and rims in or around biotite). The same is true for paragonite and margarite, which are likely to form plagioclase briefly after the entry into the amphibolite facies during the prograde path or along the decompression path. Paragonite ages are generally less precise and meet the *a priori* expectation to be equal to muscovite ages only at low metamorphic grade ($T \leq 550^{\circ}C$). At higher-grade conditions, when the P–T path crosses the paragonite-out reaction, paragonite is younger. In contrast, retrograde P–T paths for the samples studied remain within the stability field of muscovite (for metapelites and metamarls) all the way up to the surface, except near hydrothermal veins.

The age patterns of these different micas should not simply be interpreted as a revision of mica 'closure temperatures'. It is clear that micas kept at extremely high T will lose Ar. In the present case, at temperatures <600°C, the question is to what extent loss of Ar is strictly and dominantly due to diffusion (and thus can be uniquely tied to T), or to the effect of retrograde reactions, or an interplay of both processes. To answer this question, detailed petrological and thermobarometric investigations are required prior to any geochronological work. Only samples in petrological equilibrium (i.e. devoid of retrogression and inheritance) can provide reliable age information.

ACKNOWLEDGEMENTS

This work is part of a PhD thesis by J.A. at the University of Bern (Institut für Geologie). J.A. is grateful to D. Rufer for numerous discussions and his assistance in the ^{40}Ar–^{39}Ar laboratory, to Edwin Gnos for assistance in the microprobe laboratory, to O. Beyssac for the introduction to the graphite thermometry technique, and to A. Tarantola for assistance with Raman spectrometry. Help from U. Eggenberger and M. Eggimann in the XRD laboratory is greatly appreciated. We thank Vincent Serneels (University of Fribourg) for providing XRF analyses. Fruitful discussions and helpful reviews by E. Janots and M. L. Williams are acknowledged, and we are grateful to M. Sudo, F. Neubauer and two anonymous reviewers for helpful comments on this paper, and to R. Gieré for his editorial efforts.

FUNDING

The Swiss National Science Foundation provided support for this study through research projects (200020-101826 and 200020-109637), and for the electron microprobe in Bern (200021-103479/1).

SUPPLEMENTARY DATA

Supplementary Data for this paper are available at *Journal of Petrology* online.

REFERENCES

Allaz, J. (2008). Metamorphic evolution in the northern Central Alps: Linking 39Ar–40Ar dating with thermobarometry, PhD thesis, University of Bern 0, 224 pp.

Balogh, K. & Dunkl, I. (2005). Argon and fission track dating of Alpine metamorphism and basement exhumation in the Sopron

Mts. (Eastern Alps, Hungary): thermochronology or mineral growth? *Mineralogy and Petrology* **83**, 191–218.

Baumer, A., Frey, J. D., Jung, W. & Uhr, A. (1961). Die Sedimentbedeckung des Gotthard-Massivs zwischen Bleniotal und Lugnez. *Eclogae Geologicae Helvetiae* **54**, 478–491.

Belluso, E., Ruffini, R., Schaller, M. & Villa, I. M. (2000). Electron-microscope and Ar isotope characterization of chemically heterogeneous amphiboles from the Palala Shear Zone, Limpopo Belt, South Africa. *European Journal of Mineralogy* **12**, 45–62.

Berger, A., Mercolli, I. & Engi, M. (2005). The central Lepontine Alps: Notes accompanying the tectonic and petrographic map sheet Sopra Ceneri (1:100 000). *Schweizerische Mineralogische und Petrographische Mitteilungen* **85**, 109–146.

Berman, R. G. (1988). Internally-consistent thermodynamic data for minerals in the system Na_2O–K_2O–CaO–MgO–FeO–Fe_2O_3–Al_2O_3–SiO_2–TiO_2–H_2O–CO_2. *Journal of Petrology* **29**, 445–522.

Berman, R. G. (1991). Thermobarometry using multi-equilibrium calculations: a new technique, with petrological applications. *Canadian Mineralogist* **29**, 833–855.

Beyssac, O., Goffé, B., Chopin, C. & Rouzaud, J. N. (2002). Raman spectra of carbonaceous material in metasediments: a new geothermometer. *Journal of Metamorphic Geology* **20**, 859–871.

Bjørnerud, M. G., Austrheim, H. & Lund, M. G. (2002). Processes leading to eclogitization (densification) of subducted and tectonically buried crust. *Journal of Geophysical Research* **107(B10)**, 1–18.

Bucher-Nurminen, K., Frank, E. & Frey, M. (1983). A model for the progressive regional metamorphism of margarite-bearing rocks in the Central Alps. *American Journal of Science* **283(A)**, 370–395.

Chopin, C. & Maluski, H. (1980). ^{40}Ar–^{39}Ar dating of high pressure metamorphic micas from the Gran Paradiso area (Western Alps): evidence against the blocking temperature concept. *Contributions to Mineralogy and Petrology* **74**, 109–122.

Dahl, P. S. (1996). The crystal-chemical basis for Ar retention in micas: inferences from interlayer partitioning and implications for geochronology. *Contributions to Mineralogy and Petrology* **123**, 22–39.

Dalrymple, G. B. & Lanphere, M. A. (1974). $^{40}Ar/^{39}Ar$ age spectra of some undisturbed terrestrial samples. *Geochimica et Cosmochimica Acta* **38**, 715–738.

de Capitani, C. & Petrakakis, K. (2010). The computation of equilibrium assemblage diagrams with Theriak/Domino software. *American Mineralogist* **95(7)**, 1006–1016.

Di Vincenzo, G. & Palmeri, R. (2001). An $^{40}Ar/^{39}Ar$ investigation of high-pressure metamorphism and the retrogressive history of mafic eclogites from the Lanterman Range (Antartica): evidence against a simple temperature control on argon transport in amphibole. *Contributions to Mineralogy and Petrology* **141**, 15–35.

Di Vincenzo, G., Viti, C. & Rocchi, S. (2003). The effect of chlorite interlayering on ^{40}Ar–^{39}Ar biotite dating: an ^{40}Ar–^{39}Ar laser-probe and TEM investigations of variable chloritised biotites. *Contributions to Mineralogy and Petrology* **145**, 643–658.

Di Vincenzo, G., Carosi, R. & Palmeri, R. (2004). The relationship between tectono-metamorphic evolution and argon isotope records in white mica: constraints from *in situ* $^{40}Ar/^{39}Ar$ laser analysis of the Variscan basement of Sardinia. *Journal of Petrology* **45**, 1013–1043.

Dodson, M. H. (1973). Closure temperature in cooling geochronological and petrological systems. *Contributions to Mineralogy and Petrology* **40**, 259–274.

Engi, M., Todd, C. S. & Schmatz, D. R. (1995). Tertiary metamorphic conditions in the eastern Lepontine Alps. *Schweizerische Mineralogische und Petrographische Mitteilungen* **75**, 347–369.

Frank, E. (1983). Alpine metamorphism of calcareous rocks along a cross-section in the Central Alps: occurrence and breakdown of muscovite, margarite and paragonite. *Schweizerische Mineralogische und Petrographische Mitteilungen* **63**, 37–93.

Franz, G. (1977). Determination of the miscibility gap on the solid solution series paragonite–margarite by means of the infrared spectroscopy. *Contributions to Mineralogy and Petrology* **59**, 307–316.

Frey, M. (1969). *Die Metamorphose des Keupers vom Tafeljura bis zum Lukmanier-Gebiet. Beiträge zur Geologischen Karte der Schweiz, NF* **137**, 160 p.

Frey, M. (1977). Progressive low-grade metamorphism of a black shale formation, Central Swiss Alps, with special reference to pyrophyllite and margarite bearing assemblage. *Journal of Petrology* **19**, 95–135.

Frey, M. & Ferreiro Mählmann, R. (1999). Alpine metamorphism of the Central Alps. *Schweizerische Mineralogische und Petrographische Mitteilungen* **79**, 135–154.

Frey, M. & Niggli, E. (1972). Margarite, an important rock-forming mineral in regionally metamorphosed low-grade rocks. *Naturwissenschaften* **59**, 214–215.

Frey, M. & Orville, P. M. (1974). Plagioclase in margarite-bearing rocks. *American Journal of Science* **274**, 31–47.

Frey, M., Bucher, K., Frank, E. & Schwander, H. (1982). Margarite in the Central Alps. *Schweizerische Mineralogische und Petrographische Mitteilungen* **62**, 21–45.

Giletti, B. J (1974). Diffusion related to geochronology. In: Hofmann, A. W., Giletti, B. J., Yoder, H. S. & Yund, R. A. (eds) *Geochemical Transport and Kinetics. Carnegie Institution of Washington Publication* **634**, 61–76.

Glodny, J., Kühn, A. & Austerheim, H. (2008*a*). Diffusion versus recrystallization processes in Rb–Sr geochronology: Isotopic relics in eclogites facies rocks, Western Gneiss Region, Norway. *Geochimica et Cosmochimica Acta* **72**, 506–525.

Glodny, J., Kühn, A. & Austerheim, H. (2008*b*). Geochronology of fluid-induced eclogite and amphibolite facies metamorphic reactions in a subduction–collision system, Bergen Arcs, Norway. *Contributions to Mineralogy and Petrology* **156**, 27–48.

Gouzu, C., Itaya, T., Hyodo, H. & Matsuda, T. (2006). Excess ^{40}Ar-free phengite in ultrahigh-pressure metamorphic rocks from the Lago di Cignana area, Western Alps. *Lithos* **92**, 418–430.

Hammerschmidt, K. & Frank, E. (1991). Relics of high pressure metamorphism in the Lepontine Alps (Switzerland)—$^{40}Ar/^{39}Ar$ and microprobe analyses on white K-micas. *Schweizerische Mineralogische und Petrographische Mitteilungen* **71**, 261–274.

Harrison, T. M., Célérier, J., Aikman, A. B., Hermann, J. & Heizler, M. T. (2009). Diffusion of ^{40}Ar in muscovite. *Geochimica et Cosmochimica Acta* **73**, 1039–1051.

Hess, J. C., Lippolt, H. J. & Wirth, R. (1987). Interpretation of $^{40}Ar/^{39}Ar$ spectra of biotites. Evidence from hydrothermal degassing experiments and TEM studies. *Chemical Geology* **66**, 137–149.

Hetherington, C. J. & Villa, I. M. (2007). Barium silicates of the Berisal Complex, Switzerland: A study in geochronology and rare-gas release systematics. *Geochimica et Cosmochimica Acta* **71**, 3336–3347.

Jäger, E., Niggli, E. & Wenk, E. (1967). *Rb–Sr Altersbestimmungen an Glimmern der Zentralalpen. Beiträge zur Geologischen Karte der Schweiz, NF* **134** , 67 p.

Janots, E., Engi, M., Berger, A., Allaz, J. & Schwarz, O. (2008). Prograde metamorphic sequence of REE minerals in pelitic rocks of the Central Alps: implications for allanite–monazite–xenotime phase relations from 250 to 610°C. *Journal of Metamorphic Geology* **26**, 509–526.

Janots, E., Engi, M., Rubatto, D., Berger, A., Gregory, C. & Rahn, M. K. (2009). *In-situ* determination of heating rates in collisional orogeny. *Geology* **37**, 11–14.

Kogure, T. & Banfield, J. F. (2000). New insight into the mechanism for chloritization of biotite using polytype analysis. *American Mineralogist* **85**, 1202–1208.

Kretz, R. (1983). Symbols for rock-forming minerals. *American Mineralogist* **68**, 277–279.

Krumrei, T. V., Villa, I. M., Marks, M. A. W. & Markl, G. (2006). A ^{40}Ar/^{39}Ar and U/Pb isotopic study of the Ilímaussaq complex, South Greenland: Implications for the ^{40}K decay constant and for the duration of magmatic activity in a peralkaline complex. *Chemical Geology* **227**, 258–273.

Livi, K. J. T., Veblen, D. R., Ferry, J. M. & Frey, M. (1997). Evolution of 2:1 layered silicates in low-grade metamorphosed Liassic shales of Central Switzerland. *Journal of Metamorphic Geology* **15**, 323–344.

Livi, K. J. T., Ferry, J. M., Veblen, D. R., Frey, M. & Connolly, J. A. D. (2002). Reactions and physical conditions during metamorphism of Liassic aluminous black shales and marls in central Switzerland. *European Journal of Mineralogy* **14**, 647–672.

Livi, K. J. T., Christidis, G. E., Arkai, P. & Veblen, D. R. (2008). White mica domain formation: A model for paragonite, margarite, and muscovite formation during prograde metamorphism. *American Mineralogist* **93**, 520–527.

Ludwig, K. R. (2003). *User's manual for Isoplot 3.00, a geochronological toolkit for Microsoft Excel. Berkeley Geochronology Center, Special Publications* **4**, 70 p.

Milnes, A. G. (1974). Structure of the Pennine Zone (Central Alps): A new working hypothesis. *Geological Society of America Bulletin* **85**, 1727–1732.

Müller, W., Kelley, S. P. & Villa, I. M. (2002). Dating fault-generated pseudotachylytes: comparison of ^{40}Ar/^{39}Ar stepwise-heating, laser-ablation and Rb–Sr microsampling analyses. *Contributions to Mineralogy and Petrology* **144**, 57–77.

Nagel, T., de Capitani, C. & Frey, M. (2002). Isograds and *P–T* evolution in the eastern Lepontine Alps (Graubünden, Switzerland). *Journal of Metamorphic Geology* **20**, 309–324.

Onstott, T. C., Miller, M. L., Ewing, R. C., Arnold, G. W. & Walsh, D. S. (1995). Recoil refinements: Implications for the ^{40}Ar/^{39}Ar dating technique. *Geochimica et Cosmochimica Acta* **59**, 1821–1834.

Petrova, T. V., Feirreiro Mählmann, R. F., Stern, R. A. & Frey, M. (2002). Application of combustion and DTA–TGA analysis to the study of metamorphic organic matter. *Schweizerische Mineralogische und Petrographische Mitteilungen* **82**, 33–53.

Pfiffner, O. A., Ellis, S. & Beaumont, C. (2000). Collision tectonics in the Swiss Alps: insight from geodynamic modeling. *Tectonics* **19**, 1065–1094.

Probst, P. (1980). *Die Bündnerschiefer des nördlichen Penninikums zwischen Valser Tal und Passo di San Giacomo. Beiträge zur Geologischen Karte der Schweiz, NF* **153** , 63 p.

Proyer, A. (2003). The preservation of high-pressure rocks during exhumation: metagranites and metapelites. *Lithos* **70**, 183–194.

Purdy, J. & Jäger, E. (1976). *K–Ar ages on rock-forming minerals from the central Alps. Memorie dell'Istituto di Geologia dell'Università di Padova* **30**, 31 p.

Renne, P. R., Swisher, C. C., Deino, A. L., Karner, D. B., Owens, T. L. & DePaolo, D. J. (1998). Intercalibration of standards, absolute ages and uncertainities in ^{40}Ar/^{39}Ar dating. *Chemical Geology* **145**, 117–152.

Schmid, S. M., Pfiffner, O. A., Froitzheim, N., Schönborn, G. & Kissling, E. (1996). Geophysical–geological transect and tectonic evolution of the Swiss–Italian Alps. *Tectonics* **15**, 1036–1064.

Sletten, V. W. & Onstott, T. C. (1998). The effect of the instability of muscovite during *in vacuo* heating on ^{40}Ar/^{39}Ar step-heating spectra. *Geochimica et Cosmochimica Acta* **62**, 123–141.

Spicher, A. (1972). Tektonische Karte der Schweiz. Basel: Schweizerische Geologische Kommission.

Todd, C. S. & Engi, M. (1997). Metamorphic field gradients in the Central Alps. *Journal of Metamorphic Geology* **15**, 513–530.

Trommsdorff, V (1980). Alpine metamorphism and Alpine intrusions. In: Trümpy, R. (ed.) *Geology of Switzerland—a Guide-book, part A: An Outline of the Geology of Switzerland.* Basel: Wepf, pp. 82–87.

Villa, I. M. (1998*a*). Direct determination of ^{39}Ar recoil distance. *Geochimica et Cosmochimica Acta* **61**, 689–691.

Villa, I. M. (1998*b*). Isotopic closure. *Terra Nova* **10**, 42–47.

Villa, I. M. (2001). Radiogenic isotopes in fluid inclusions. *Lithos* **55**, 115–124.

Villa, I. M. (2004). Geochronology of metamorphic rocks. *Periodico di Mineralogia (Special Issue 2: A showcase of the Italian research in metamorphic petrology)* **73**, 259–271.

Villa, I. M. (2006). From nanometer to megameter: Isotopes, atomic-scale processes, and continent-scale tectonic models. *Lithos* **87**, 155–173.

Villa, I. M (2010). Disequilibrium textures vs equilibrium modelling: geochronology at the crossroads. In: Spalla, M. I., Marotta, A. M. & Gosso, G. (eds) *Advances in Interpretation of Geological Processes. Geological Society, London, Special Publications* **332**, 1–15.

Villa, I. M. & Buettner, A. (2009). Chronostratigraphy of Monte Vulture Volcano (southern Italy): secondary mineral microtextures and ^{39}Ar–^{40}Ar systematics. *Bulletin of Volcanology* **71**, 1195–1208.

Villa, I. M. & Puxeddu, M. (1994). Geochronology of the Larderello geothermal field: new data and the 'closure temperature' issue. *Contributions to Mineralogy and Petrology* **115**, 415–426.

Villa, I. M., Grobéty, B., Kelley, S. P., Trigila, R. W. & Wieler, R. (1996). Assessing Ar transport paths and mechanisms in the McClure Mountains hornblende. *Contributions to Mineralogy and Petrology* **126**, 67–80.

Villa, I. M., Hermann, J., Müntener, O. & Trommsdorff, V. (2000). ^{39}Ar/^{40}Ar dating of multiply zoned amphibole generations (Malenco, Italian Alps). *Contributions to Mineralogy and Petrology* **140**, 363–381.

Villa, I. M., Ruggieri, G., Puxeddu, M. & Bertini, G. (2006). Geochronology and isotope transport systematics in a subsurface granite from the Larderello–Travale geothermal system (Italy). *Journal of Volcanology and Geothermal Research* **152**, 20–50.

Viti, C., Di Vincenzo, G. & Mellini, M. (2004). Thermal transformations in laser-heated chloritized annite. *Physics and Chemistry of Minerals* **31**, 92–101.

Wijbrans, J. R. & McDougall, I. (1986). ^{40}Ar/^{39}Ar dating of white micas from an Alpine high-pressure metamorphic belt on Naxos (Greece): the resetting of the argon isotopic system. *Contributions to Mineralogy and Petrology* **93**, 187–194.

Zimmermann, J. L. (1970). Contribution à l'étude de la déshydratation et de la libération de l'argon des micas. *Geochimica et Cosmochimica Acta* **34**, 1327–1350.

APPENDIX: ANALYTICAL METHODS

^{40}Ar–^{39}Ar stepwise heating; instrument setup

Samples were irradiated either in the TRIGA reactor at Pavia University (Italy) or at McMaster University

(Hamilton, Canada). Fast neutron flux was monitored by use of MMhb standard hornblende (523·1 ± 4·6 Ma; Renne *et al.*, 1998) intercalated between analysed samples. Interference and production factors for Ca, Cl and K were those used by Belluso *et al.* (2000). Ar isotope analyses were performed at the Institut für Geologie, Universität Bern, using an all-metal extraction line attached to a double-vacuum resistance oven and a thermocouple on the external part of the crucible (Belluso *et al.*, 2000). Furnace blanks yielded an atmospheric composition in all series. Typically, ^{40}Ar blanks ranged from 3·0 pl min^{-1} at 400°C to 4·5 pl min^{-1} at 700°C and 14·3 pl min^{-1} at 1000°C. Errors shown in the data tables, in the age spectra and in the correlation diagrams of Figs 7–10 are given as 1σ. They propagate the uncertainties on blank correction, interfering reaction, air calibration, J-factor determination, and the in-run statistics. Isochemical and plateau ages discussed in the text and shown in Figs 7–10 are given as 2σ. All weighted averages were calculated with Isoplot (Ludwig, 2003). After a pre-cleaning stage at 400°C for at least 15 min, the mineral separate was heated at intervals of 10–100°C from *c.* 500°C to more than 1400°C. When samples were analysed successively and when crucible and resistance conditions were similar, the inter-sample temperature bias is believed to be better than ±5°C. This is the case for the four samples ALu0601, -03 and APi0601, -03 analysed in immediate succession. The uncertainty in absolute temperatures between different series of analyses is conservatively estimated as ±30°C.

Owing to changes in the argon extraction line over the last few years (breakdown of multiplier and later replacement by a new one), analyses presented here were obtained during three independent series with slightly different analytical setup: Ar-A included samples ALu0306 and APi0301; Ar-B, samples AMo0409 and AMo0410; Ar-C, samples ALu0601, ALu0603, APi0601 and APi0603. The Ar extraction and the cleaning system remained identical. The atmospheric contribution from the oven was variable from 7% to 68% for the major steps (usually < 30%), and significantly higher for analyses of nearly pure paragonite and margarite separates (61–84%). Spectrometer background has slightly changed: 17 ± 8 pl ^{40}Ar, 2·2 ± 0·9 pl ^{39}Ar, 0·47 ± 0·13 pl ^{38}Ar, 0·93 ± 0·23 pl ^{37}Ar and 0·68 ± 0·22 pl ^{36}Ar. In series Ar-B, all masses (including 38 and 37) were measured on the Faraday cup. In series Ar-A and Ar-C, masses 40, 39 and 36 were measured on the Faraday cup and masses 39 to 36 on a 19 Cu–Be dynode MasCom electron multiplier. Detection limits are 0·5 fl on Faraday measurement and one order of magnitude lower on the multiplier. In series Ar-A, the electron multiplier was used in analogue mode; in series Ar-C, it was used in pulse-counting mode. The signal was amplified through a pulse preamplifier WMT PAD06 set at 40 ns dead time. A threshold value of −4·5 mV was selected to reduce electronic noise. Values were corrected for dead time according to the following equations (unpublished MasCom User's Manual): $a = C \cdot e^{C \cdot D}$; $b = C \cdot e^{a \cdot D}$; $X = C \cdot e^{b \cdot D}$, where C is the measured count rate (in counts per second), D is the dead time (in seconds) and X is the corrected count rate.

In vacuo Ar release from micas and mica mixtures

If a mica mixture has to be analysed for ^{40}Ar–^{39}Ar dating, notably muscovite with paragonite or margarite, we must first examine whether the *in vacuo* Ar release of each component is different. The Ar release rate from biotite and three white micas (given as per cent release per unit time and unit temperature difference) is shown in Supplementary Data Fig. 1. Steps of degassing below 600°C usually do not pertain to micas, and mostly contribute an insignificant percentage of the total ^{39}Ar and ^{40}Ar* (Supplementary Data Table 2). Fluid inclusions (notably in quartz or kyanite) similarly affect only steps below 600°C or at melting (Villa, 2001, and references therein): large fluid inclusions decrepitate at low temperature during stepwise heating analyses, whereas nanometer-sized ones may never decrepitate before melting. A higher Cl (and often Ca) characterizes the release of gas from fluid inclusions. The 'fusion' step of each analysis (*c.* 1400–1500°C) always contains a very minor amount of ^{40}Ar* and ^{39}Ar, and ensures that the mica has released its argon entirely.

Pure muscovite separates show two distinct Ar release patterns. In samples from the Lucomagno and Piora areas, two distinct and narrow peaks exist for ^{40}Ar*, ^{39}Ar and ^{38}Ar, around 790 and 1050°C (Supplementary Data Fig. 1a). In samples from higher metamorphic grade, a single large peak is present around 850°C and is slightly asymmetric toward higher temperature (Molare; Supplementary Data Fig. 1b). Sletten & Onstott (1998) proposed a two-stage decomposition to explain the double peak: in the first stage, major dehydration and delamination of muscovite occurs; in the second stage, stronger ionic bonds are broken, and Ar is released from dehydroxylated muscovite. Sletten & Onstott suggested a dependence of Ar release upon grain size in muscovite. Our study fails to confirm this conclusion, as different grain-size fractions yield similar Ar release patterns (e.g. ALu0601; Supplementary Data Fig. 1a). Hetherington & Villa (2007) had argued against delamination as the predominant cause of Ar and Xe release from Ba-muscovite. We note that explanations of the unimodal or bimodal release may require prior characterization of polytype modifications as a function of the chemical composition or of metamorphic grade, but no quantitative explanation is attempted here.

Biotite releases Ar in a large range between 600 and 1150°C (Supplementary Data Fig. 1c and d). Two peaks

are typically visible and may correspond to two decomposition stages: first, delamination and dehydration of mica; second, the dissociation of stronger ionic bonds with the formation of new phases at high temperature (spinels, olivine and Si–Al-glass; Zimmermann, 1970; Di Vincenzo *et al.*, 2003; Viti *et al.*, 2004). In the Piora and Lucomagno areas, the Ar release profile reveals two peaks around 760 and 970°C (Supplementary Data Fig. 1c), and the temperature interval is even narrower in biotite from Lucomagno Pass (800 and 920°C). In the Molare area, the two peaks are further apart (*c.* 720 and 1010°C; Supplementary Data Fig. 1d). Biotite chemistry is likely to induce such difference in Ar release patterns, with a first Ar release peak at higher temperature in Mg-rich biotite (800°C in ALu0306; 0·29 Fe*) compared with Fe-richer biotite (720°C, in AMo0409 and -10; 0·39 and 0·45 Fe*). Zimmermann (1970) had observed a later release of structural water in phlogopite, which is consistent with its higher thermal stability owing to shorter and stronger interatomic bonds, proxied by ionic porosity (Dahl, 1996). This is corroborated by our observations. A slight increase in metamorphic grade and a change in biotite composition (Fig. 3b) probably also affect bond strength and therefore control the thermal peak of Ar release rates.

Compared with the muscovite degassing profile (Supplementary Data Fig. 1a), the release of Ar from margarite is remarkably distinct. XRD results from a first white-mica separate of the margarite-bearing metamarl ALu0306 reveal only traces of muscovite (~1–3%) with a large amount of margarite and quartz (Mrg-rich), whereas a second separate contains most probably <10% muscovite (Mrg ± Ms). Both separates show $^{40}Ar^*$ and ^{39}Ar release between 700 and 1150°C (Supplementary Data Fig. 1e), whereas the ^{37}Ar peak is present only at high temperature between 900 and 1100°C (Supplementary Data Fig. 1f). A double peak is visible in the Mrg ± Ms separate resulting from the strong influence of the minor muscovite component in this mineral separate (compare Supplementary Data Fig. 1a and e). In contrast, only a broad ^{39}Ar peak is identified in the Mrg-rich separate, resulting from the degassing of muscovite (double peak around 800 and 1100°C) and margarite (single release around 950°C). High-temperature steps are thus mixtures of ^{39}Ar contributed both by margarite and muscovite, whereas low-temperature steps derive solely from muscovite.

Paragonite contains only small amounts of K and Ca. This renders the interpretation of Ar-release profiles more difficult in mineral separates containing muscovite and minor paragonite, as muscovite dominates the ^{39}Ar release (Supplementary Data Fig. 1g). A direct comparison of muscovite and paragonite release is possible in ALu0603, where the coarser fraction is enriched in paragonite whereas the finer one is richer in muscovite. In general, the highest ^{37}Ar release rate is observed between 750 and 950°C, and is variable from sample to sample (Supplementary Data Fig. 1h).